

²D. N. Payton and W. M. Visscher, Phys. Rev. 154, 802 (1967); 156, 1032 (1967); 175, 1201 (1968).

³R. J. Elliott and D. W. Taylor, Proc. Roy. Soc. (London) A296, 161 (1967).

⁴D. W. Taylor, Phys. Rev. 156, 1017 (1967).

⁵J. M. Rowell and W. L. McMillan, in *Superconductivity*, edited by R. D. Parks (M. Dekker, New York, 1969).

⁶J. M. Rowell, W. L. McMillan, and P. W. Anderson,

Phys. Rev. Letters 14, 633 (1965).

⁷J. R. Schrieffer, *Theory of Superconductivity* (Benjamin, New York, 1964).

⁸J. G. Adler and J. E. Jackson, Rev. Sci. Instr. 37, 1947 (1966).

⁹D. W. Taylor (private communication).

¹⁰These results are quoted in Ref. 3.

¹¹D. J. Scalapino, J. R. Schrieffer, and J. W. Wilkins, Phys. Rev. 148, 263 (1966).

PHYSICAL REVIEW B

VOLUME 6, NUMBER 1

1 JULY 1972

Phonon Fluorescence in Superconductors and the Propagation Characteristics of High-Frequency Phonons in Ge:Sb and Al₂O₃:V³⁺

R. C. Dynes and V. Narayanamurti

Bell Telephone Laboratories, Murray Hill, New Jersey 07974

(Received 20 January 1972)

We present a detailed account of phonon generation by superconducting tunnel junctions (Sn-I-Sn) and by Sn and Pb_{0.5}Tl_{0.5} films pumped by a heat pulse. The spectrum and propagation characteristics of the generated phonons is studied through the resonance absorption by Sb-donor levels in uniaxially compressed Ge. At all values of generator power (up to a few watts) the emitted phonons show a large density at a value of energy equal to the superconducting energy gap (2Δ). In contrast, the spectrum emitted by a constant heater is shown to be in quantitative agreement with the blackbody-radiation model. The experiments show that the mean free path of longitudinal and transverse phonons in the superconductor changes discontinuously when $\hbar\omega = 2\Delta$. Theoretical calculations show that significant reabsorption of phonons of energy $> 2\Delta$ results in a nonlinear buildup of the intensity of the 2Δ phonons. The propagation characteristics of these phonons in Ge:Sb show a frequency and polarization dependence in excellent agreement with the Griffin-Carruthers theory of resonance-fluorescence phonon scattering by donor levels. The magnetic field tunability of the generated 2Δ phonons in Sn is utilized to study the ground state of V³⁺ in Al₂O₃. Transverse phonons of energy 1.02 meV propagating along the *c* axis are resonantly absorbed as expected according to theory.

I. INTRODUCTION

The primary motivation for high-frequency phonon-propagation research is its application to a variety of problems at thermal frequencies. At frequencies above about 5×10^{10} Hz several interesting effects become observable. For example, the energy gap (2Δ) of most superconductors lies in the region of 0.4 to 4 meV ($\sim 10^{11}$ to 10^{12} Hz). Thus, high-frequency phonon-propagation studies might reveal important parameters about the electron-phonon interaction in superconductors and their relationship to other measurements. Also, the energy levels of a variety of defects in insulators and semiconductors lie in the range of thermal-phonon frequencies. In many cases the levels of interest are strongly coupled to the strain and hence phonon excitation may be a more fruitful (and possibly simpler) method to study such levels than conventional far-infrared photon absorption. In addition, the problem of phonon-defect interaction is of interest in itself. Finally, lattice anharmonicity and dispersion (in the acoustic modes)

become important in many solids (and liquid helium) at frequencies of 10^{11} to 10^{12} Hz. Thus, it is clear that monochromatic-phonon-propagation experiments at high frequencies are potentially of interest to the current theories of heat transport (thermal-phonon lifetimes), electron-phonon interactions, and nonlinear parameters in a variety of different materials.

In this paper we present a detailed account of our work^{1,2} on the spectrum of phonons generated by (a) thin-film superconducting tunnel junctions³ (Sn-I-Sn) and (b) by superconducting (Sn and Pb_{0.5}Tl_{0.5}) films pumped by a heat pulse. The spectra and propagation characteristics of the generated phonons are studied through the observation of resonance absorption by Sb-donor levels in uniaxially compressed Ge and by time-of-flight techniques. We show that the spectrum consists of a narrow band of phonons centered at the superconducting energy gap 2Δ . Furthermore, the emitted-phonon frequency is tuned by application of a magnetic field parallel to the plane of the film. This tunability is used to study the ground-

state splitting of V^{3+} ions in Al_2O_3 . Our measurements provide some answers to the questions discussed in the previous paragraph. In particular, we present (a) strong evidence for the discontinuous change in phonon lifetime when the phonon energy becomes greater than the superconducting energy gap and (b) we show that one can get detailed information about the modal, directional, and frequency dependence of the phonon-defect interaction for two different cases in a very direct way.

Other techniques, besides that discussed above, have been used for phonon-propagation spectroscopy in the past. Thermal-conductivity⁴ and more recently heat-pulse^{5,6} measurements have been successfully used to study resonant phonon scattering by impurities, but with a resolution comparable to $k_B T$. Morton and Rosenberg⁷ and Walton⁸ have achieved higher resolution by measuring the change in thermal conductivity as a function of magnetic field in crystals doped with paramagnetic impurities; the phonons in resonance with the Zeeman splitting of the spins "burn a hole" in the blackbody spectrum and hence a higher resolution is achieved. Shiren,⁹ Anderson and Sabisky,¹⁰ Channin *et al.*,¹¹ and Renk and Deisenhofer¹² have used paramagnetic and paraelectric impurities for monochromatic-phonon generation and, particularly, detection. These techniques, though narrow band, are not generally applicable to a wide class of materials because of the problem of acoustically bonding one crystal to another. On the other hand, Brillouin scattering¹³ is a general technique, with good frequency and directional resolution, but with presently available lasers it is limited to microwave frequencies while the frequencies of interest in our experiment are typically at least an order of magnitude higher. Finally, conventional ultrasonic techniques are also limited to frequencies of the order of 10^{10} Hz because coherent piezoelectric detection of very short-wavelength acoustic waves requires perfection of sample geometries to an atomic scale.¹⁴ In our experiment the problem of geometrical perfection is circumvented by using thin-film superconducting tunnel junctions as incoherent quantum generators and detectors. Furthermore, the excellent acoustical contact (with solids) made by evaporated thin films enables one to do a time-of-flight measurement at high frequencies in analogy with the usual pulsed-microwave ultrasonic experiment.

The paper is divided into four major parts. Section II contains the theoretical and experimental background on heat-pulse propagation in solids, phonon generation, and detection using superconducting tunnel junctions and contains the results of calculations on the lifetime of high-frequency phonons in superconductors. A summary is given

of what is known about the phonon-defect interaction for the systems of concern to us in this work. In this section we attempt to develop a unified view, especially since a large number of different fields are involved.

Section III describes the experimental techniques. Particular emphasis is given to details, which are not normally found in the literature, and which we believe will be useful to other investigators.

Section IV summarizes our experimental results. In this section we also give a brief discussion of the dynamical processes occurring in a superconductor under intense excitation and point to future directions of study.

II. THEORETICAL AND EXPERIMENTAL BACKGROUND

In this section we briefly review the salient features of heat-pulse propagation in solids, phonon generation, and detection using superconducting thin films and the selection rules governing the phonon-defect interaction for the cases of interest.

A. Heat-Pulse Propagation in Solids

The properties of thermal phonons in many solids have recently been studied by the heat-pulse method.^{15,16} In this method the phonons are generated by passing a submicrosecond current pulse through a heater film (typically constantan) evaporated onto one end of the sample under study and are detected at the other end (after a time of flight determined by the mode of propagation) by means of a thin-film superconducting bolometer. The shapes and intensities of the received heat pulses depend strongly on the phonon mean free path Λ (relative to the sample length L), and we discuss three distinct cases below.

1. Case of No Scattering ($\Lambda \gg L$)

In this regime the heat pulse travels purely ballistically and arrives at the detector at times corresponding to rectilinear propagation of longitudinal and transverse sound. The heat-pulse properties¹⁷ are determined by the rate at which the phonon power is transmitted (per unit area) from the heater to the sample and is given by a Stephan-Boltzmann-type radiation law

$$\frac{P(T_h, T_s)}{A} = \frac{V_i^2}{R} \int_0^{\omega^D} g(\omega, T_h, T_s) d\omega,$$

with

$$g(\omega, T_h, T_s) = \frac{\hbar\omega^3}{2\pi^2} \left[\left(\frac{t_L^{hs}}{(v_L^h)^2} + \frac{2t_T^{hs}}{(v_T^h)^2} \right) (e^{\hbar\omega/k_B T_h} - 1)^{-1} - \left(\frac{t_L^{sh}}{(v_L^s)^2} + \frac{2t_T^{sh}}{(v_T^s)^2} \right) (e^{\hbar\omega/k_B T_s} - 1)^{-1} \right]. \quad (1)$$

In (1) T_h is the heat-pulse temperature; T_s is the

ambient temperature of the sample; V_i is the input heater voltage; R is the heater resistance; v_L^h , v_T^h , v_L^s , v_T^s are velocities of longitudinal and transverse sound in the heater and sample; and t_L^{hs} , t_T^{hs} , t_L^{sh} , t_T^{sh} are acoustic transmission coefficients from heater to sample and sample to heater. Several attempts have been made to calculate and measure these coefficients.¹⁷ In the perfect-coupling blackbody-radiation model^{15,17} the entire thermal energy radiated by the heater is transmitted to the solid under study and the transmission coefficients (which are related to each other by the "principles of detailed balance") have a value equal to unity. If the constant metal film were not in excellent thermal contact with the crystal, typical pulse powers of several watts or more would heat the film ($d \approx 500 \text{ \AA}$) to many thousand degrees and burn it out. For a ballistic heat-pulse experiment to work the thermal relaxation time of the metal film to the solid must be much less than the pulse duration. Thus, if the thermal energy (heat) is perfectly coupled to the crystal under study, one end of the crystal gets heated up during the application of the pulse. The volume heated up is $A\bar{v}^s\delta t$, where A is the contact area, \bar{v}^s is the average sound velocity, and δt is the pulse duration. The heat-pulse temperature is then, given by

$$\frac{P(T_h, T_s)}{A} = \frac{V_i^2}{R} = \frac{4\pi^5}{15\hbar^3} k_B^4 \left(\frac{1}{(v_L^s)^2} + \frac{2}{(v_T^s)^2} \right) (T_h^4 - T_s^4) = \sigma(T_h^4 - T_s^4), \quad (2)$$

where

$$\frac{3}{(\bar{v}^s)^2} = \frac{1}{(v_L^s)^2} + \frac{2}{(v_T^s)^2}.$$

Throughout the above discussion we are assuming the Debye model, i. e., $k_B T_h \ll \hbar\omega_D$, and that the sample is isotropic. Even in the absence of polarization-dependent scattering the absolute intensity of the different polarizations will depend strongly on orientation of the sample due to channeling or focusing of the radiated-phonon energy due to the elastic anisotropy.¹⁸ For simplicity we are neglecting such focusing effects here but will come back to it later when we discuss the absolute intensities of our observed pulses in Sec. IV A.

In Eq. (1), $g(\omega, T_h, T_s)$ specifies the frequency spectrum of phonons in the heat pulse. If the power supplied to the heater is small, i. e., $T_h \approx T_s$, then $g(\omega, T_h, T_s)$ has its maximum at $\hbar\omega_{\max} \approx 3.8k_B T_s$, and one essentially does a sophisticated thermal-conductivity experiment with time-resolution capability. Thus Eqs. (1) and (2) reduce to

$$V_i^2/R = 4\sigma \Delta T/T_s^3 \quad (3)$$

as expected, where we have assumed that $\Delta T = T_h - T_s$ is small compared to T_s . Under these conditions (and assuming that the bolometer is a

good, broad-band energy detector) the detector signal is proportional to V_i^2 and T_s^{-3} .

If the power supplied to the heater is large, $T_h \gg T_s$, and Eq. (1) simply becomes

$$V_i^2/R = \sigma T_h^4. \quad (4)$$

The phonon-frequency distribution is now characterized by a high temperature T_h and is independent of the ambient temperature T_s of the crystal. This enables one to vary the phonon frequencies and the ambient temperature independently, something which cannot be done in the conventional thermal-conductivity experiment. The maximum in the phonon-frequency spectrum now occurs at $\hbar\omega_{\max} \approx 2.8k_B T_h$. It is important to emphasize here that in the ballistic regime the heat-pulse temperature is not a well-defined quantity, and the concept of a "pulse temperature" is merely used to specify the frequency spectrum via the blackbody-radiation formula. The actual temperature rise at the detector end may be quite small due to geometrical losses which are large, for example, if the heater and detector are small in size. Thus the problem here is analogous to that of radiation from the stars whose frequency spectrum is characterized by a high "temperature" but with a continuously decreasing radiation energy density via some geometrical "dilution function." Thus the signal at the bolometer end can still be proportional to V_i^2 but the heat-pulse temperature (which specifies the frequency distribution) will be proportional to the square root of the input voltage V_i .

2. Case of Weak Scattering ($\Lambda \approx L$)

If the mean free path $\Lambda \approx L$, then the ballistic pulse is attenuated somewhat and the scattered energy ends up in a weak diffusive pulse. This is the regime which will be of primary concern to us in this paper since we are interested mainly in the modal and directional-propagation characteristics of the phonon pulses.

Assuming that only single-scattering events take place, the unscattered power is damped exponentially¹⁹ and Eq. (1) for the power in the ballistic pulse reduces to

$$P(T_h, T_s)/A = \int_0^{\omega_D} g(\omega, T_h, T_s) e^{-L/\Lambda(\omega, T_s)} d\omega \neq \sigma(T_h^4 - T_s^4) \neq V_i^2/R. \quad (5)$$

Thus the power transmitted is no longer given by (3) or (4) and one has to invoke a specific model for $\Lambda(\omega, T_s)$ and convolute the Planck integral (5) to get the dependence of the transmitted power in the ballistic pulse. Or conversely, by careful measurements of the power dependence of the ballistic-pulse amplitude one can, by curve fitting, obtain the frequency and temperature dependence of the phonon mean free path $\Lambda(\omega, T_s)$. In Eq. (5)

we have not assumed any explicit polarization dependence of $\Lambda(\omega, T_s)$, however, (5) can very simply be generalized to take this into account by breaking up $g(\omega, T_h, T_s)$ and $\Lambda(\omega, T_s)$ into individual polarization components. Such a procedure is valid because the time of overlap of the longitudinal and transverse pulses is small if the pulse width is much less than the transit time as is usually the case in our experiments.

3. Case of Strong Scattering ($\Lambda \ll L$)

If the phonon mean free path is very short, the ballistic pulse is rapidly attenuated and almost all of the signal ends up in the diffusion pulse. The ratio²⁰ of the amplitude of the ballistic pulse (I_B) to that of the diffusion pulse (I_D), at the time of arrival of the ballistic pulse is given by²⁰

$$\frac{I_B}{I_D} \left(t = t_B = \frac{L}{v_B} \right) = \frac{(\delta t)t_B}{8\tau^2}, \quad (6)$$

where δt is the width of the input pulse and $\tau = \Lambda/v$ is the relaxation time.

In the limit $\tau \rightarrow 0$, the shape of the diffusion pulse is a Gaussian,²⁰ i. e.,

$$\lim I_D(L, t) = \frac{\Delta T}{2} \frac{\delta t}{(4\pi t\tau)^{1/2}} e^{-t^2/4t\tau} \quad \text{as } \tau \rightarrow 0, \quad (7)$$

where

$$t \gg t_B.$$

In (7) ΔT the temperature rise is assumed small. In all of the discussion above Λ is assumed to be governed by resistive-scattering processes only. If "normal" processes are dominant the heat pulse can travel as a true "temperature wave" or "second sound" as has been observed by others.²¹ Such second-sound propagation will not be of concern to us and hence is not discussed further.

B. Phonon Generation and Detection Using Superconducting Tunnel Junctions

In this section we consider briefly the properties of single-particle tunneling in superconducting tunnel junctions as phonon generators and detectors. In all of this discussion we are referring to a symmetric junction (superconductor-insulator-superconductor).

1. Phonon Generation

If a voltage $V > 2\Delta/e$ is applied to a superconducting tunnel junction, the injected high-energy quasiparticles, according to Tewordt,^{22,23} decay primarily by a two-step process involving incoherent phonon emission. The probability for phonon emission has been shown^{24,25} to be negligibly small. The first step consists of a relaxation in time τ_T to energy Δ (measured with respect to the Fermi level) and simultaneous emission of a single

phonon. For the excitation energies of interest Tewordt has shown that two-phonon emission has a negligible effect on particle decay in comparison to single-phonon emission. The relaxation phonons will, however, possess a continuous energy spectrum, ranging from 0 to $eV - 2\Delta$ reflecting the BCS distribution of injected quasiparticles²⁶ and/or the phonon density of states $F(\omega)$ in the superconductor.²⁷ In the second step two quasiparticles at the gap edge recombine and emit in time τ_R a "monochromatic" phonon of energy 2Δ .

The relaxation and recombination lifetimes τ_T and τ_R have been measured experimentally²⁸ in the case of Al and have the respective values of $\approx 10^{-9}$ and $\approx 10^{-6}$ sec at 0.37 °K. At comparable reduced temperatures these times are believed to be considerably shorter for the stronger-coupled superconductors, such as Pb and Sn which are of interest in this work. Assuming a spherical Fermi surface and an average electron-phonon coupling constant derived from high-temperature resistivity Schrieffer and Ginsberg²⁵ and Rothwarf and Cohen²⁹ have calculated a value of the order of 10^{-8} sec for τ_R for the case of Pb at 1.4 °K. The small value of this lifetime is necessary for studies involving time-resolved phonon spectroscopy.

Thus for an arbitrary bias voltage V the spectrum of generated phonons should consist of a monochromatic recombination peak at 2Δ and a continuous spectrum of relaxation phonons with a cutoff at $\hbar\omega_{ph} = eV - 2\Delta$. The width of the monochromatic peak, neglecting gap anisotropy, is due to a velocity threshold effect which causes the recombination process and should yield a Q of typically 10^5 . The intensity of the monochromatic peak must increase linearly with generator current (for $2\Delta < eV < 4\Delta$) since each injected quasiparticle contributes to one recombination phonon of energy 2Δ . For $eV \geq 4\Delta$ the intensity of the 2Δ peak must increase nonlinearly for two reasons: (i) Additional 2Δ phonons are created during the relaxation process and (ii) due to significant reabsorption of phonons of energy $> 2\Delta$ within the generator films by pair breaking, additional 2Δ phonons will be created when the secondary quasiparticles recombine to form Cooper pairs. That such reabsorption of high-energy phonons is the dominant mechanism for the film thickness of interest here was suspected by Kinder, Laszmann, and Eisenmenger.²⁶ We recently showed experimentally^{1,2} that this is true and we discuss it in greater detail later in this paper. Theoretical calculations which show the nonlinear buildup in the intensity of 2Δ phonons are discussed in Sec. II C.

2. Phonon Detection

As mentioned briefly above and discussed in greater detail later, the mean free path of phonons

of energy $\hbar\omega \geq 2\Delta$ is extremely short ($\lesssim 1000 \text{ \AA}$) in superconductors such as Sn and Pb and hence highly sensitive detection of high-frequency phonons is possible with thin films of these materials.

A tunnel-junction detector works in a manner complementary to the tunnel-junction generator discussed above. The detector is current biased in the voltage range of thermally excited quasiparticle tunneling ($0 < eV < 2\Delta$) and at a point where dV/dI is a maximum. Phonons with an energy $\geq 2\Delta$ are strongly absorbed and break Cooper pairs. The increase in number of excited quasiparticles causes a large drop in the voltage for a constant-current-biased junction.

For film thicknesses and temperatures of interest the junction is believed to be perfectly transparent for phonons $\hbar\omega < 2\Delta$ and perfectly black for phonons $\hbar\omega > 2\Delta$, with the width of the absorption edge at 2Δ being determined by gap anisotropy. In Sec. II C we provide quantitative estimates on the absorption coefficient for high-frequency phonons in a superconductor.

C. Heat Pulses and the Attenuation of High-Frequency Phonons in a Superconductor

One of the outstanding successes of the BCS theory³⁰ of superconductivity has been the successful explanation of the temperature dependence of the ultrasonic attenuation in superconductors for frequencies $\hbar\omega \ll 2\Delta$. According to the BCS theory the chief difference in the ultrasonic attenuation in a superconductor compared to a normal metal arises from the coherence effects associated with the pairing. If the attenuation is normalized to the normal state, all terms excepting the terms involving coherence effects in the matrix element drop out. The net result is

$$\frac{\alpha_S}{\alpha_N} = \frac{1}{\hbar\omega} \int \left(\frac{EE' - \Delta^2}{EE'} \right) \operatorname{Re} \left(\frac{EE'}{[(E^2 - \Delta^2)(E'^2 - \Delta^2)]^{1/2}} \right) \times [f(E) - f(E')] dE, \quad (8)$$

where in the weak-coupling limit $\Delta = \Delta_0$ and is real. In (8) α_S and α_N are the attenuations in the superconducting and normal states, respectively, $E' = E + \hbar\omega$, and $f(E) = (e^{E/k_B T} + 1)^{-1}$ is the Fermi function. In the usual ultrasonic case of $\hbar\omega \ll \Delta$ the coherence factor cancels out the density-of-states factor and we get

$$\alpha_S/\alpha_N = 2f(\Delta). \quad (9)$$

If, however, the phonon energy $\hbar\omega$ is not small compared to 2Δ then (8) can be written in the form

$$\frac{\alpha_S}{\alpha_N} = \frac{2}{\hbar\omega} \int_{\Delta}^{\infty} \frac{EE' - \Delta^2}{[(E^2 - \Delta^2)(E'^2 - \Delta^2)]^{1/2}} [f(E) - f(E')] dE$$

$$- \frac{1}{\hbar\omega} \int_{\Delta - \hbar\omega}^{-\Delta} \frac{EE' - \Delta^2}{[(E^2 - \Delta^2)(E'^2 - \Delta^2)]^{1/2}} \times [f(E) - f(E')] dE. \quad (10)$$

The first term in (10) corresponds to the scattering of a quasiparticle by a phonon and is absent at $T = 0 \text{ }^\circ\text{K}$. The second term corresponds to a creation of a pair of quasiparticles by the decay of a phonon and is usually referred to as the pair-breaking term. The pair-breaking term occurs at all temperatures as long as $\hbar\omega \geq 2\Delta(T)$.

The lifetimes of the quasiparticles and phonons in a superconductor for $\hbar\omega \sim 2\Delta$ were first calculated by Tewordt²² and at about the same time by Privorotskii.³¹ These calculations were quantitatively extended by Bobetic³² who used numerical-integration methods. The results are summarized in Figs. 1(a) and 1(b) where we show the frequency dependence at a fixed reduced temperature ($t = T/T_c$) and the temperature dependence for a fixed frequency. It is clear that there is a large discontinuous change in absorption when $\hbar\omega = 2\Delta(T)$. The magnitude of the discontinuous jump is given by

$$\delta(\alpha_S/\alpha_N) = \frac{1}{2}\pi [1 - 2f(\Delta(T))], \quad (11)$$

and at very low temperatures [$\hbar\omega \cong 2\Delta(0)$] has the value of $\frac{1}{2}\pi$. The infinite slope of the absorption edge arises from the square-root density-of-states factors occurring in (10) and is to be contrasted with the linear rise in absorption at the corresponding energy threshold in electromagnetic absorption.³³ It is clear from Eq. (11) and Fig. 1 that at elevated temperatures ($t \gtrsim \frac{1}{2}$), $\delta(\alpha_S/\alpha_N)$ decreases due to the additional absorption by thermally excited quasiparticles. Nevertheless, in the isotropic model the gap edge $\hbar\omega = 2\Delta(T)$ continues to be an infinitely sharp threshold.

The magnitude of the change in α_S for $\hbar\omega \geq 2\Delta$ when compared with $\hbar\omega \ll 2\Delta$ is even more striking. At temperatures of the order of $1.2 \text{ }^\circ\text{K}$ the change in absorption coefficients at the gap edge corresponds to a change in value of the order of 10^4 and 10^3 in the phonon mean free path for Pb and Sn. The *absolute* magnitude of the absorption coefficient at the gap edge is somewhat more difficult to estimate. This depends on a precise knowledge of the magnitude of α_N . These values are unknown experimentally for the cases of tin and lead at the frequencies of interest. If one extrapolates the very low-frequency ultrasonic measurements for longitudinal modes of Mason and Bommel³⁴ to a frequency of $5 \times 10^{11} \text{ Hz}$ according to theory,³⁵ one obtains a mean free path of the order of 10^{-5} cm .

So far we have not considered any explicit polarization dependence. In the BCS expression for the *ratio* α_S/α_N the polarization terms cancel. According to the classical theory of ultrasonic atten-

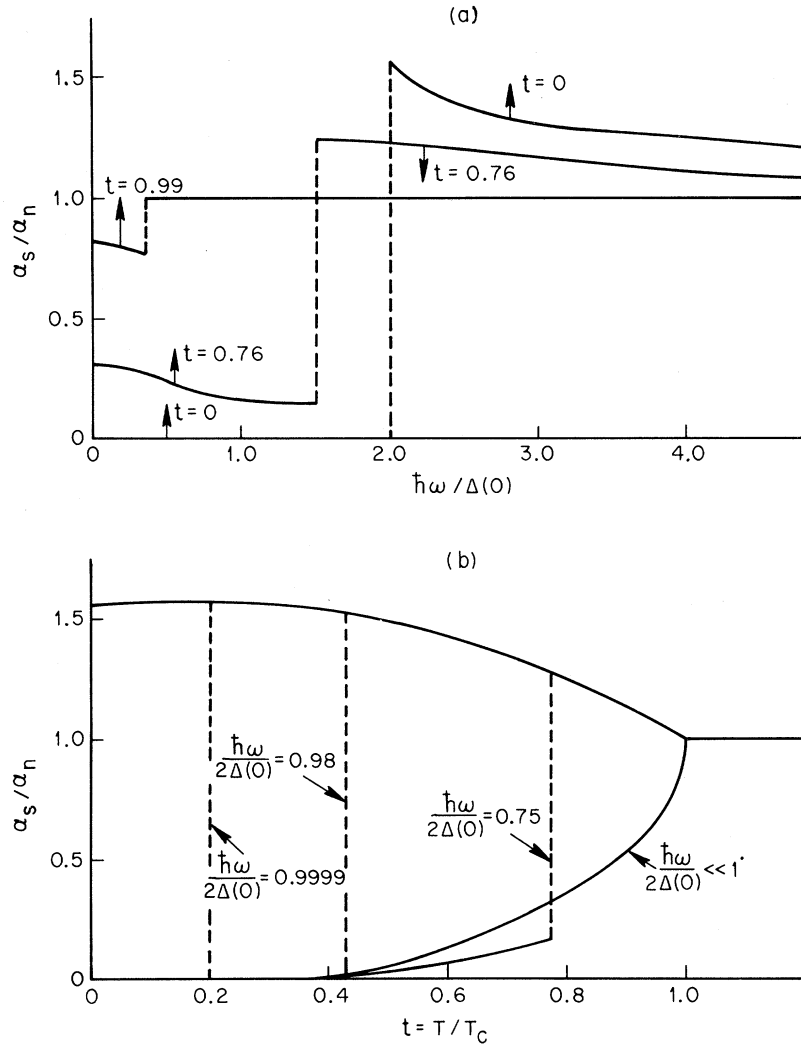


FIG. 1. Ratio of attenuation α_S/α_N is plotted as a function of phonon energy $\hbar\omega$ for fixed reduced temperature $t = T/T_c$. In (b) α_S/α_N is plotted as a function of t for fixed $\hbar\omega$.

uation in metals by Mason³⁵ and Pippard³⁶ the value of α_N should increase linearly with frequency for longitudinal waves at high frequencies. The attenuation for transverse waves at high frequencies is extremely small and independent of frequency. This strong polarization dependence is also predicted by the quantum theory of the electron-phonon interaction (in the free-electron theory) as long as one considers "normal" (N) processes only. In such a process $\vec{q} = \vec{\kappa} - \vec{\kappa}'$ (\vec{q} is the phonon-momentum, and $\vec{\kappa}$ and $\vec{\kappa}'$ are the electron momenta before and after scattering), and since the interaction³⁷ goes as $(\vec{\kappa} - \vec{\kappa}') \cdot \hat{e}_\lambda$ where \hat{e}_λ is the polarization of the sound wave, it is zero for transverse phonons. In an umklapp (U) process, however, the electron and phonon momenta are no longer perpendicular for the transverse phonons and the interaction is nonzero. It is important to point out here that the precise magnitudes of the N and U processes will depend on the details of the band structure of

the material but on the basis of a free-electron picture umklapp processes can be significant, as shown by Rothwarf and Cohen²⁹ for the particular case of Pb. They found the matrix elements for the two polarizations to be comparable, and the chief difference was due to the larger density of states of transverse phonons (typically a factor of 5 or 10 for most materials). As we shall see later, this strong coupling to both polarizations is confirmed by our measurements.

We now consider briefly the experimental situation. Due to the difficulty of generating high-frequency phonons, very few measurements exist on the attenuation of such phonons in normal and superconducting metals. The highest reported measurements are those of Fagen and Garfunkel³⁸ at 9.3 GHz in Al and the very recent work of Garfunkel, Lue, and Pike³⁹ in Mo and Cd at the same frequency. At this frequency $\hbar\omega/\Delta(0)$ is ~ 0.3 to 0.5 for Mo and Cd and in these materials a change

in slope in the absorption at a temperature 0.02°K below T_c was observed and attributed to pair breaking. The large finite slope was explained by a large gap anisotropy ($\sim 30\%$). The measured value of α_N was 16 dB for a $23\text{-}\mu\text{m}$ -thick Cd sample. Since the energy gaps of Sn and Pb are, respectively, 8 and 18 times larger than that of Cd and also because of the much stronger electron-phonon coupling, our earlier estimate of about 10^{-5} cm for the mean free path for gap-frequency phonons appears reasonable.

That the mean free path for such phonons must be extremely short was also indicated by recent measurements by one of us⁴⁰ on heat-pulse transmission through single-crystal lead. At an ambient crystal temperature of 1.3°K and heater temperatures of 1.5 and 3.4°K phonon mean free paths of $\sim 10^{-1}$ and 10^{-2} cm were obtained. For $T_H = 3.4^\circ\text{K}$ the dominant phonon frequency was ~ 200 GHz. From the ambient temperature dependence of the attenuation it was concluded that a substantial part of the attenuation was due to thermally excited quasiparticles. This yields a value of $\sim 10^{-6}$ cm for 200-GHz phonons in the normal state of Pb.

The entire discussion in this section concerning the discontinuous change in lifetime by orders of magnitude for gap-frequency phonons immediately leads one to ask the following question: Can one use superconducting films to generate phonons with a sharp upper cutoff and perhaps a large density at 2Δ by simply pulsing them or by pumping them with a broad-band source such as a heat pulse? In Sec. IV we will show experimentally that this is indeed possible. In this section we merely present the results of theoretical calculations on the generated spectrum.

Consider a heat-pulse incident on a superconducting film. We assume that both the duration and rise time of the pulse are faster than the recombination lifetime for the levels of excitation of interest in this work. All those phonons in the heat pulse, with an energy $\hbar\omega > 2\Delta$, will have a high scattering rate for pair breaking. The resulting quasiparticles excited above the gap edge will emit a relaxation phonon plus a recombination phonon necessarily of energy 2Δ . If the relaxation phonon has energy greater than 2Δ , it will be reabsorbed and pair break. The repeated quasiparticle relaxations (according to the BCS density of states) and their subsequent recombination with other quasiparticles to form Cooper pairs, will result in a nonlinear buildup of the intensity of the 2Δ phonons as mentioned briefly in Sec. II B 1. In addition, there will be a low-energy contribution of relaxation phonons. The intensity ratio of the 2Δ to the low-energy phonons is determined by the pump power (heater temperature), the value of

2Δ and the linewidth of the recombination phonons.

In Fig. 2 we show the effect of the repeated foldings of the BCS ultrasonic-attenuation ratio,¹⁰ which was computed numerically for a heater temperature of 5°K (a typical value for many of our experiments). The calculations were done for Sn ($2\Delta = 1.2$ meV), $\text{Pb}_{0.5}\text{Tl}_{0.5}$ ($2\Delta = 1.7$ meV), and Pb ($2\Delta = 2.8$ meV). The spectrum of recombination phonons was assumed to be a Lorentzian line with a width at half-maximum equal to 5% of the energy gap. Under these conditions the peak at 2Δ is largest for Sn since the number of phonons with energy $> 2\Delta$ in the heat pulse is largest for the film with the smallest gap.

Finally, in Fig. 3 we show the effect of varying the heater temperature for a Sn generator with a fixed linewidth of 5% of the energy gap. Here again the nonlinear increase of the intensity of the 2Δ phonons is evident.

It is important to note that these calculations were performed for an ambient temperature $T = 0^\circ\text{K}$. This then assumes no thermally excited quasiparticles. In addition, we have ignored the effect of a large density of particles (Fermi statistics) due to the actual injection process. These

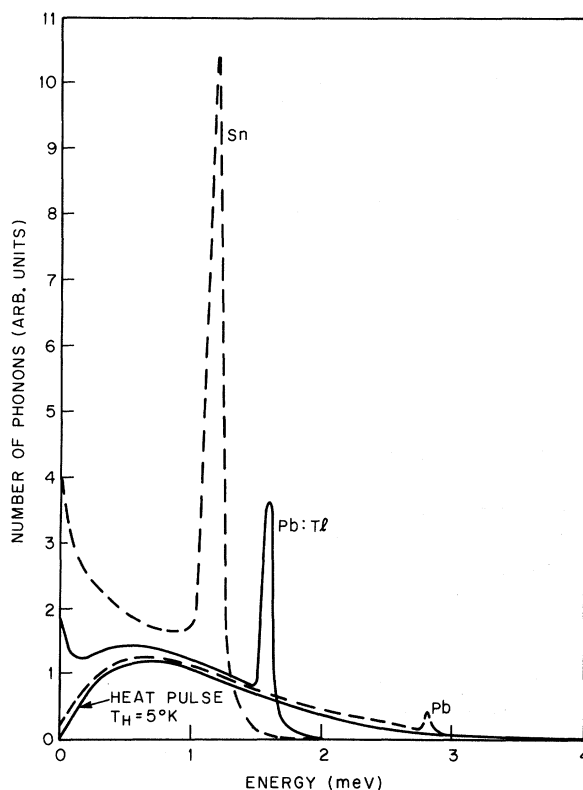


FIG. 2. Theoretically expected phonon-fluorescence spectrum for Sn, $\text{Pb}_{0.5}\text{Tl}_{0.5}$, and Pb for an incident-heat-pulse temperature of 5°K . Linewidth of recombination phonons was assumed to be 5% of the energy gap.

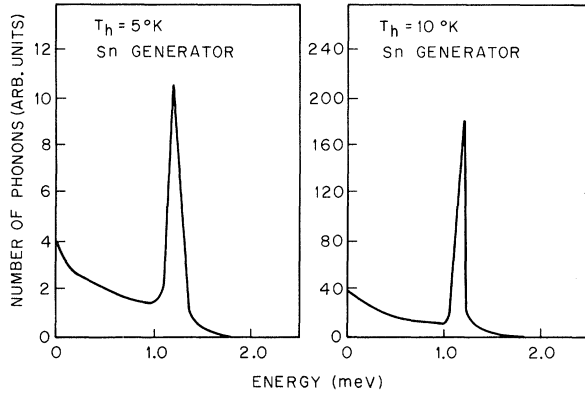


FIG. 3. Theoretical fluorescence spectrum of Sn generator for two values of T_h . Note the change in vertical scale.

points will be considered again in Sec. IV. Also, it has been assumed that the superconducting film is "black" (i. e., all phonons $\hbar\omega > 2\Delta$ are absorbed).

In summary, it is clear that if the absorption coefficient for phonons of energy $> 2\Delta$ is high, then one can indeed pump a superconductor with a blackbody source of phonons and expect to observe the system emit a discrete spectrum with a large peak at 2Δ , the superconducting energy gap. Due to the strong similarity to optical pumping of energy levels with tungsten lamps, we have termed this process "phonon fluorescence." In Sec. IID we consider the possibility of tuning this fluorescence spectrum by means of a magnetic field.

D. Superconducting Film in a Magnetic Field

The problem of the behavior of a superconducting film in a parallel magnetic field H was first considered by Ginzburg and Landau⁴¹ in terms of a phenomenological theory for the order parameter ψ . They showed that if the thickness d of the film is much less than the London penetration depth λ , then the order parameter goes continuously to zero as the field is increased going through a second-order phase transition at the critical field H_c . If, on the other hand, $d \gg \lambda$, then ψ decreases continuously to a critical value ψ_c (which is a function of position in the film) at which point it abruptly drops to zero in a first-order transition.

The Ginzburg-Landau equations were later re-derived by Gor'kov⁴² from the microscopic theory of superconductivity. He showed that under certain conditions the order parameter $\psi(H)$ is proportional to the energy gap $\Delta(H)$ of the BCS theory. Explicit expressions, assuming that the energy gap was independent of position in the film, have been given by Douglass.^{43,44} Figure 4 gives a theoretical plot of the gap parameter on the basis of the Ginzburg-Landau theory for various values of the

ratio d/λ . In the limit $d/\lambda \ll 1$ we find

$$\left(\frac{\Delta(H)}{\Delta(0)}\right)^2 = 1 - \left(\frac{H}{H_c}\right)^2. \quad (12)$$

The behavior of Al films in parallel magnetic fields was first studied by Giaever and Megerle⁴⁵ who showed that $\Delta(H)$ decreased monotonically with field. Later measurements by Meservey and Douglass⁴⁴ on Al films and by Collier and Kamper⁴⁶ on Sn films showed that the data could be quantitatively interpreted on the basis of the Ginzburg-Landau theory of a field-dependent energy gap.

The above discussion is valid in the so-called "clean" limit (coherence length \gg penetration depth). If the coherence length is \ll penetration depth, the problem is more complicated as was first investigated by Maki⁴⁷ and de Gennes.⁴⁸ They showed that the effect of a magnetic field on a "dirty" superconductor (i. e., one where the electron mean free path is considerably reduced due to scattering with nonmagnetic impurities) is analogous to the problem of a superconductor containing magnetic impurities considered by Abrikosov and Gor'kov.⁴⁹ For the latter problem, Abrikosov and Gor'kov showed that the energy gap goes to zero at a critical impurity concentration (91%) but the order parameter remains finite over a finite temperature range. Such "gapless" superconductivity has been well established experimentally and appears to be a quite general phenomenon.

In the Maki-de Gennes theory the square of the magnetic field is analogous to the magnetic impurity concentration of the Abrikosov-Gor'kov theory. Thus, a "dirty" superconductor in a magnetic field becomes "gapless" at $(H/H_c)^2 = 0.91$. In addition,

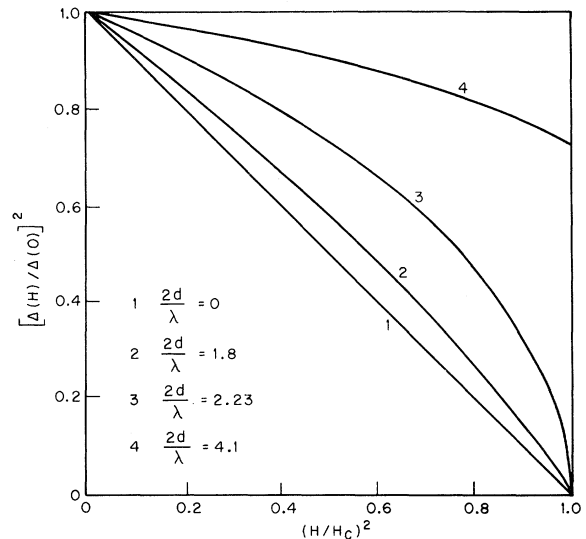


FIG. 4. Theoretically expected variation of energy gap as a function of field for different values of the ratio $2d/\lambda$. $2d$ is the film thickness. Ginzburg-Landau theory.

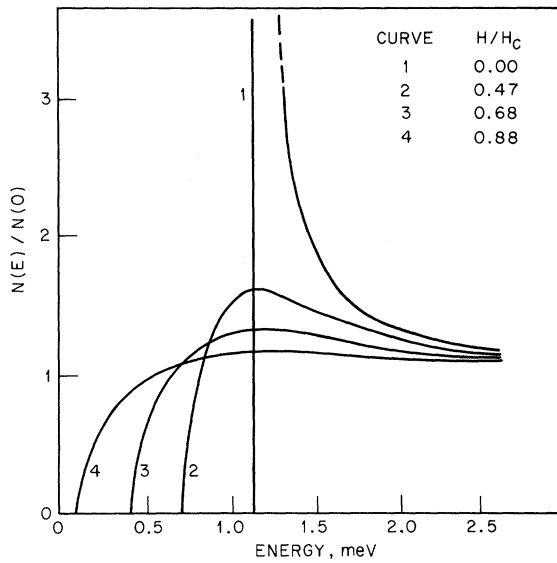


FIG. 5. Density of excitations as a function of energy for different values of H/H_c for a "dirty" superconductor. After Skalski *et al.*, Ref. 50.

for $H \neq 0$, the density of states broadens out in a manner similar to that calculated by Skalski *et al.*⁵⁰ for the case of a superconductor containing magnetic impurities. This broadening of the density of the excitations and the disappearance of the BCS singularity for a thin dirty superconductor in a parallel magnetic field is illustrated in Fig. 5. This behavior has been quantitatively verified for the case of dirty Sn and In films.^{51,52}

It is important to point out here that even in the dirty limit the gap edge remains reasonably sharp and decreases monotonically with field (see Fig. 5). The maximum in the density of states, however, remains close to the zero-field value. Thus, the phonons generated by a dirty superconducting film may still possess a reasonably well-defined frequency peak (if there is significant reabsorption of high-energy phonons and, as discussed in Sec. IIC, the gap edge controls the frequency of generated phonons).

In summary, great care has to be taken in parametrizing the films if one wishes to quantitatively specify their behavior in a magnetic field. Since in our experiment we actually measure the frequency of emitted phonons we will in this paper choose the phenomenological approach and give a recipe for determining this frequency in terms of the I - V characteristics of the tunnel junctions in a magnetic field.

E. Phonon-Defect Interaction

In this section we consider in some detail the nature of the phonon-defect interaction for the two

cases of interest; Ge:Sb and $\text{Al}_2\text{O}_3:\text{V}^{3+}$.

Case (i): Sb Donors in Uniaxially Compressed Ge. The scattering of phonons by bound donor electrons in Si and Ge has been an interesting problem ever since the early thermal-conductivity measurements of Fagen *et al.*⁵³ and Carruthers *et al.*⁵⁴ It was shown that this scattering was far too strong to be explained by the usual mechanisms of impurity scattering (isotope, strain field⁵⁵) and that at very low temperatures the conductivity increases much faster than the usual T^3 . Keyes⁵⁶ first proposed that the strong scattering of phonons arose from the large effect of strain on the energy of an electron in a hydrogenlike donor state. Later Griffin and Carruthers⁵⁷ explained the thermal conductivity of n -Ge in great detail on the basis of an elastic resonance-fluorescence scattering model. Recently Kwok⁵⁸ has extended the problem to include inelastic scattering processes to explain the microwave-ultrasonic-attenuation measurements of Pomerantz.⁵⁹ In this section we will consider these models in greater detail but first we discuss briefly the effect of static strain on the energy levels.

In the effective-mass approximation⁶⁰ the ground state of a donor in Ge is fourfold degenerate because of the four equivalent $\langle 111 \rangle$ conduction minima. Due to the valley-orbit interaction⁶¹ caused by the impurity potential (this causes a breakdown in the effective-mass theory because the s -like ground-state wave function has a finite amplitude in the region close to the donor nucleus where the assumption of a Coulomb potential of the form $V = e/Kr$ is no longer valid) this degeneracy is partially lifted into a singlet ground state $A_1(S)$ and an excited triplet state which are separated by the "chemical shift" of $4\Delta_c$. In Ge, the value of $4\Delta_c$ is 0.32 meV for Sb, 2.83 meV for P, and 4.23 meV for As. The small value of $4\Delta_c$ and the consequent much larger effects of strain, which are important both for the large static-stress tunability of the levels and the strong electron-phonon interaction, were the principal reason for choosing Sb donors in this study.

The effect of uniaxial stress on the donor energy levels was first calculated by Price.⁶¹ In the case of Ge a uniaxial stress along $[111]$ destroys the degeneracy of the four-conduction-band minima which causes a splitting of the triplet state into a singlet $A_1(T)$ and a doublet $E(T)$. The shift of the first valley along $[111]$ is, by deformation-potential theory, -3ϵ ; similarly the other three valleys along $[1\bar{1}\bar{1}]$, $[\bar{1}1\bar{1}]$, and $[\bar{1}\bar{1}1]$ are raised by an amount ϵ , with

$$\epsilon = (E_u/9C_{44})X, \quad (13)$$

where E_u is the shear deformation-potential constant, C_{44} is one of the elastic stiffness constants,

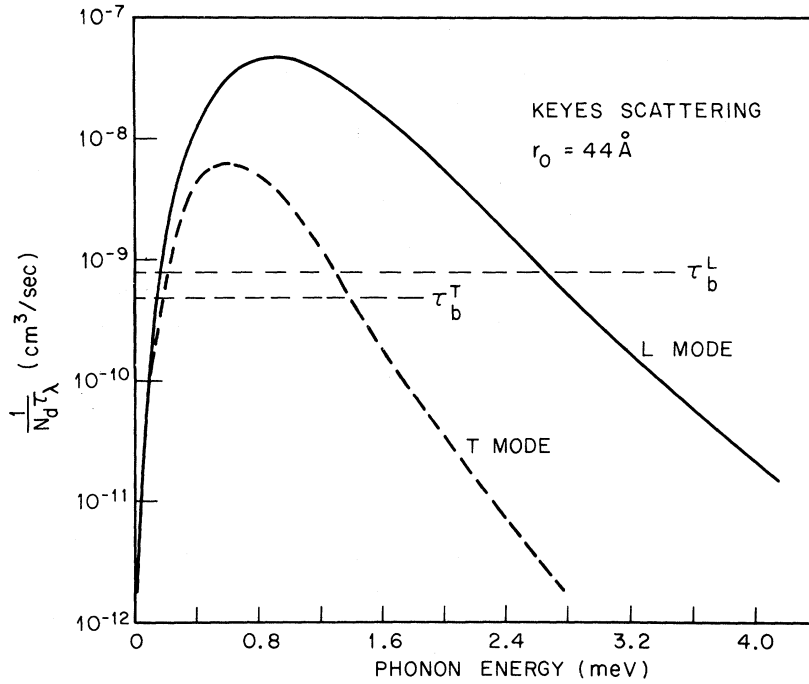


FIG. 7. $1/N_d\tau_\lambda$ (Keyes) plotted as a function of phonon energy. $r_0=44 \text{ \AA}$, $E_u=16 \text{ eV}$, $4\Delta_c=0.32 \text{ meV}$. For an explanation of the lines marked τ_b^T and τ_b^L see text.

wave functions of the individual states [see Eq. (9) of Kwok's paper] we find that for $\vec{q} \parallel [110]$, the L mode induces transitions from $A_1(S)$ to $A_1(T)$, the FT mode from $A_1(S)$ to $E(T)$, and the ST mode remains uncoupled. These selection rules are completely verified by our experiment.

The above theory of Hasegawa was used by Keyes to explain the anomalous thermal conductivity of n -Ge. He considered an interaction with the static-strain field of the donor which gives the usual ω^4 dependence to the scattering. An additional frequency dependence arises when the phonon wavelength is less than the mean radius r_0 of the localized state, causing the average strain and hence the interaction to approach zero. This sharp cutoff was used by Keyes to explain the steepness of the thermal conductivity curve. The expression for $1/\tau$ given by Keyes has the form

$$\frac{1}{\tau_\lambda}(\text{Keyes}) = \frac{N_d}{\pi\rho^2} \left(\frac{E_u^2}{4\Delta_c} \right)^2 \frac{2\omega^4}{3^4 5} \left(\frac{2}{3\bar{v}_L} + \frac{1}{\bar{v}_T} \right) D^\lambda F^\lambda(q). \quad (21)$$

In Eq. (21) N_d is the concentration of donors, ρ the density, ω the circular frequency in rad/sec, \bar{v}_L and \bar{v}_T average longitudinal and transverse sound velocities, D^λ an anisotropy factor having average values of $\frac{4}{5}$ for L modes and $\frac{3}{5}$ for T modes, and $F(q)$ is the cutoff factor of Eq. (16).

In Fig. 7 we plot $(1/\tau_\lambda)(\text{Keyes})$ for a single donor as a function of phonon energy for the parameters relevant to Ge:Sb. The dashed lines τ_b^T and τ_b^L correspond to lines when the ballistic arrival times

for the two polarizations equal the relaxation times $\tau_\lambda(\text{Keyes})$ for a concentration of 2×10^{15} donors cm^{-3} . We assume the sample is of length 3.5 mm. Figure 7 shows the q cutoff of the $F^\lambda(q)$ term quite clearly. The relaxation times for high frequencies differs as much as two orders of magnitude between the L and T modes.

In most of our experiments we keep the phonon frequency fixed but vary the splitting $4\Delta_c$. In Fig. 8 we plot $1/N_d\tau$ as a function of $4\Delta_c$ for a fixed phonon energy of 1.2 meV ($2\Delta_{Sn}$). We have again drawn lines corresponding to τ_b^T and τ_b^L . It is clear from this figure that the T mode should interact very weakly for $4\Delta_c \gtrsim 0.5 \text{ meV}$ and the L -mode cutoff should be $\sim 2.2 \text{ meV}$. We have assumed for simplicity in this calculation that r_0 remains unchanged. The wave-function calculations of Fritzsche⁶¹ show that this is a reasonable approximation.

The Keyes model, discussed above, proved quite successful in describing the relaxation time for phonons obtained from thermal-conductivity measurements. It could, for example, explain not only the strength of the donor scattering in n -Ge but also the species dependence through its dependence on $4\Delta_c$. However, it was clear that for phonon frequencies in the neighborhood of the valley-orbit splitting the perturbative static-strain-field calculation of Keyes must break down. Griffin and Carruthers⁵⁷ treated the problem of scattering of phonons by donors in analogy with the problem of resonance-fluorescence scattering of light by

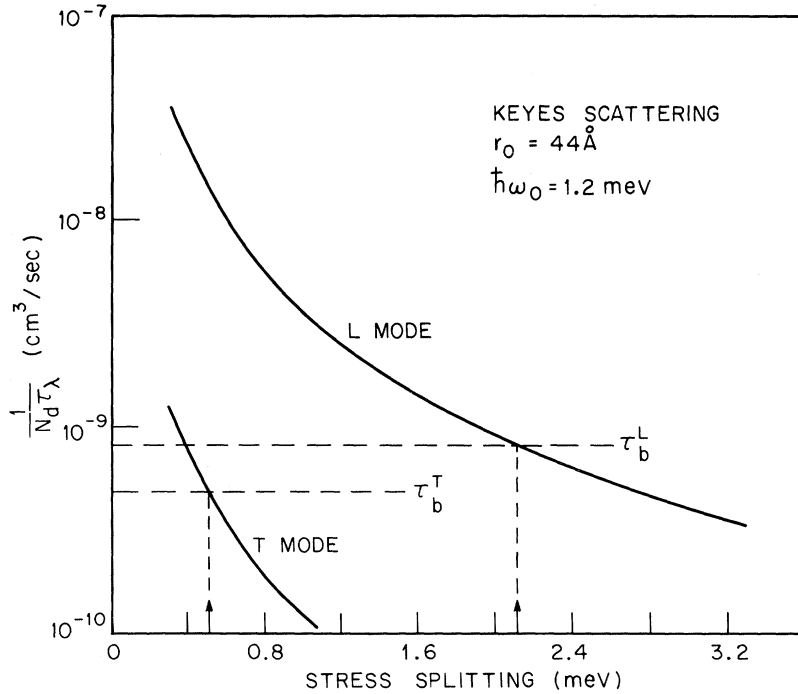


FIG. 8. Plot of $1/N_d\tau_\lambda$ (Keyes) as a function of stress splitting for Ge:Sb. Incident phonon energy $\hbar\omega_0=1.2$ meV.

atoms. The expression for such resonance scattering was calculated to be

$$\frac{1}{\tau_{q,\lambda}} = \frac{N_d}{3^4 \pi \rho^2} \frac{E_d^4 H_\lambda \omega^4}{(4\Delta_c)^2} \left(\frac{(4\Delta_c)^4}{[(\hbar\omega)^2 - (4\Delta_c)^2]^2 + \gamma^2 (\hbar\omega)^6} \right) \times \left[\frac{F^2(q, \lambda)}{v_\lambda^2} \left(\frac{F^2(q, L)}{v_L^5} + \frac{3}{2} \frac{F^2(q, T)}{v_T^5} \right) \right] B(T). \quad (22)$$

In (22), $B(T)$ is a population factor which is close to unity for our temperatures. H_λ is an angular factor which is equal to $\frac{43}{225}$ for L modes and $\frac{32}{225}$ for T modes. The term $\gamma^2(\hbar\omega)^6$ in the resonance denominator was not in the original Griffin-Carruthers expression but is used here to describe the finite lifetime effects as pointed out by Pohl.⁶⁸ The original Griffin-Carruthers expression unphysically diverged at resonance. We see in addition to the resonance terms of the large curly brackets, the \bar{q} cutoff predicted by Keyes also exists in this expression.

We have calculated (22) as a function of ω for fixed $4\Delta_c$ and as a function of $4\Delta_c$ for a fixed ω . As a function of ω the curves obtained were similar to curves in Figs. 2 and 3 of the Griffin-Carruthers paper, namely, a resonance at $4\Delta_c$ riding on a Keyes background. The strength of the resonance relative to the background depends strongly on the value of γ . In Fig. 9 we plot $1/N_d\tau(q, L)$ as a function of $4\Delta_c$ for $\omega=1.2$ meV for two values of γ . The curve $\gamma=0.1$, corresponds to a linewidth of about 0.35 meV. It is clear that even for such

large linewidths the resonance dominates. In Fig. 10 we plot $1/N_d\tau(q, \lambda)$ as a function of stress splitting for $\omega=1.2$ meV and $\gamma=0.03$ for L and T modes. The L - and T -mode relaxation times are comparable, and the mean free paths ($\Lambda=v\tau$) are consequently almost equal.

In summary, the chief difference between the Griffin-Carruthers and Keyes models is the presence of a resonance for $\omega=4\Delta_c$. The resonance term dominates the scattering for typical linewidths of the order of a few percent of the frequency. In addition, the Keyes model predicts an order-of-magnitude stronger L -mode than T -mode scattering while the resonance expression predicts that the two scatterings should be comparable in magnitude.

Case (ii): V^{3+} ions in Al_2O_3 . The V^{3+} ion has two d electrons, and the effect of crystalline fields on the 3F free-ion state is shown in Fig. 11. In our experiment only the 3A_2 ground state is of interest since the trigonal splitting⁶⁷ is believed to be ~ 0.15 eV. The 3A_2 state is split, due to the combined action of the trigonal field and spin-orbit interaction, into a state $M_s=0$ and an excited state $M_s=\pm 1$. This splitting has been studied by far-infrared absorption⁶⁸ and is equal to 1.02 meV.

Dreyfus and Zadworny⁶⁹ and deGoer⁷⁰ have studied the effect of V^{3+} ions on the thermal conductivity of Al_2O_3 . Recent experiments on the ultrasonic paramagnetic resonance at 9 GHz by Guermeur *et al.*⁷¹ on the $\Delta M=\pm 2$ transitions show that this ion is fairly strongly coupled to the lat-

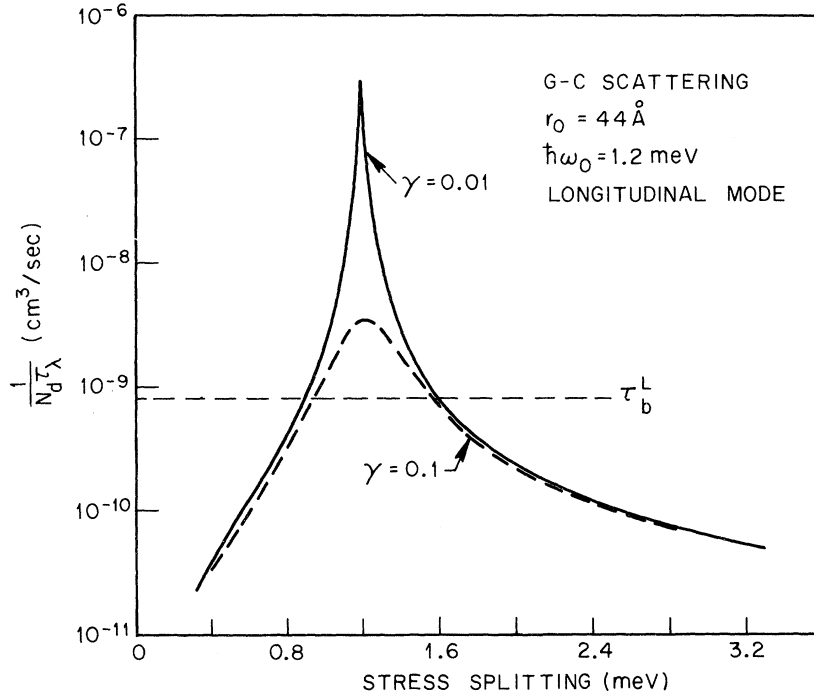


FIG. 9. $1/N_d\tau_\lambda$ (Griffin-Carruthers) plotted as a function of stress splitting for two values of the linewidth γ . Longitudinal mode. Phonon energy $\hbar\omega_0 = 1.2$ meV.

tice. Previous experiments by one of us⁶ on heat pulses in $\text{Al}_2\text{O}_3:\text{V}^{3+}$ showed that at concentrations of ~ 500 ppm this ion caused a noticeable reduction in ballistic pulses of high enough temperature to induce $\Delta M_s = \pm 1$ transitions. This indicated a mean free path of the order of the sample length (~ 1 cm). The absorption was confirmed through the selection rules. These selection rules could be derived from the theory of spin-phonon coupling which has been considered for a variety of cases by several authors.^{72,73} For an ion with an effective spin $S > \frac{1}{2}$ the dynamic spin-phonon Hamiltonian is quadratic in spin operators and is of the form

$$\mathcal{H}' = \sum_{ijkl} G_{ij,kl} \epsilon_{ij} S_k S_l, \quad (23)$$

where $G_{ij,kl}$ is the magnetoelastic tensor, ϵ_{ij} is the strain matrix, and the S_k , S_l are spin operators.

In the Al_2O_3 lattice, the V^{3+} ion (which replaces the Al^{3+}) is surrounded by six oxygens forming a distorted octahedron, the symmetry of which is C_3 . The threefold axis is parallel to the c axis (chosen as O_z) and the a axis (chosen as O_x) is the twofold axis of symmetry. The C_3 site symmetry reduces the number of independent G constants. For this case the G tensor is given by

$$G = \begin{pmatrix} G_{11} & G_{12} & -\frac{1}{2}G_{33} & G_{14} & G_{15} & G_{16} \\ G_{12} & G_{11} & -\frac{1}{2}G_{33} & -G_{14} & -G_{15} & -G_{16} \\ -(G_{11} + G_{12}) & -(G_{11} + G_{12}) & G_{33} & 0 & 0 & 0 \\ G_{41} & -G_{41} & 0 & G_{44} & G_{45} & G_{46} \\ -G_{46} & G_{46} & 0 & -G_{45} & G_{44} & G_{41} \\ -G_{16} & G_{16} & 0 & -G_{15} & G_{14} & \frac{1}{2}(G_{11} - G_{12}) \end{pmatrix}. \quad (24)$$

By using the fact that the trace⁷³ of \mathcal{H}' is zero one gets the additional relation $G_{31} = -(G_{11} + G_{12})$ and $G_{13} = -\frac{1}{2}G_{33}$.

For phonons propagating along O_z the only non-zero deformations are e_{zz} (L mode) and $e_{zx,zy}$ (T mode). Since the $\Delta M_s = \pm 1$ transitions are induced

by terms involving $S_z S_x$, $S_z S_y$, we find that L modes along O_z cannot induce $\Delta M_s = \pm 1$ transitions, while T modes can do so with a transition probability proportional to G_{44}^2 and G_{45}^2 . If the site symmetry were C_{3v} , G_{45} would be zero.⁷³ In the case of Al_2O_3 , G_{45}^2 is expected to be much smaller than

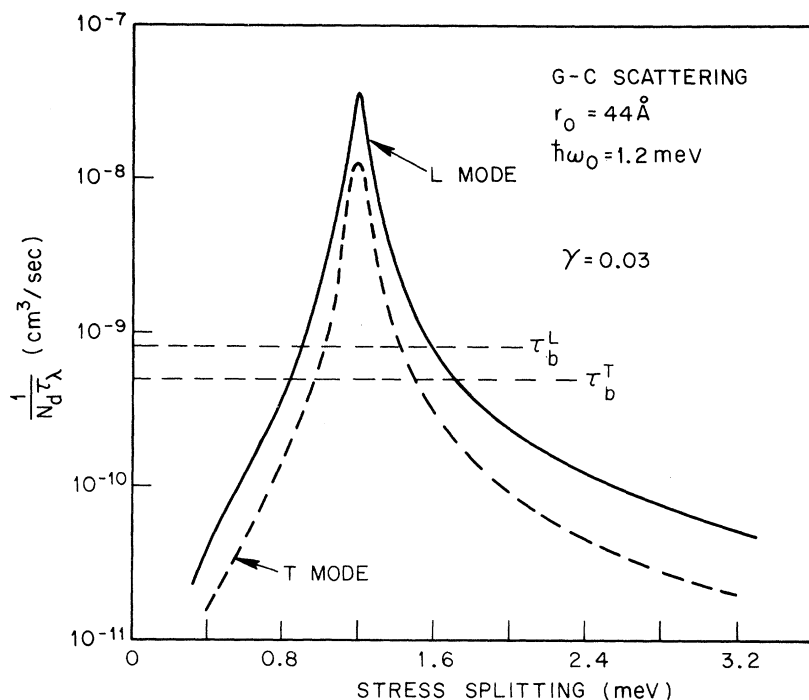


FIG. 10. Griffin-Carruthers scattering as a function of stress splitting for L and T modes. Phonon energy $\hbar\omega_0 = 1.2$ meV. Note that the mean free paths $v_\lambda\tau_\lambda$ are almost identical in this model.

G_{44}^2 .

The absorption coefficient at resonance should therefore be given approximately by⁷³

$$\alpha_T = \frac{\pi n g(v)}{\hbar \rho v_T^2} |G_{44}|^2, \quad (25)$$

where $g(v)$ is the shape of the absorption line, n the number of ions per cm^3 in the ground state, ρ the density of the crystal, and v_T the transverse sound velocity.

III. EXPERIMENTAL TECHNIQUES

Many of the experimental aspects of this work have been mentioned previously but elaboration and clarification of the more salient points seems necessary. In this section we shall stress the technique which appeared most difficult in practice, and in an attempt to assist future investigators in avoiding these problems we emphasize the errors that can be and have been made.

By far, the most important aspect of sample preparation was the smoothness and cleanliness of the surface of the crystal onto which the thin films were evaporated. It was found that if any irregularities (dust, scratches, metal particles, etc.) were observed on microscopic investigation of the surface, the quality of the tunnel junctions or heat-pulse generators was reduced. Although this generation technique appeared to be sufficiently general to be applied to any sort of solid where the phonon mean free path Λ was \sim the sample dimensions, it was absolutely necessary that the sur-

faces be free from irregularities down to the resolution of an optical microscope. Otherwise, tunnel junctions displayed characteristics related to pin-hole shorts through the oxide, heaters were shorted to the superconductors to be pumped, entire films and contacts lifted off very easily during the cool-down period, and the success ratio was generally very low. On the other hand, when the surfaces were well prepared, all other things being equal, the percentage of successful devices was quite high.

All the tunnel junctions considered in this work were of the thin-film Sn-I-Sn type, where I is a plasma-grown oxide of the bottom Sn film. For details of the art of tunnel-junction manufacture,

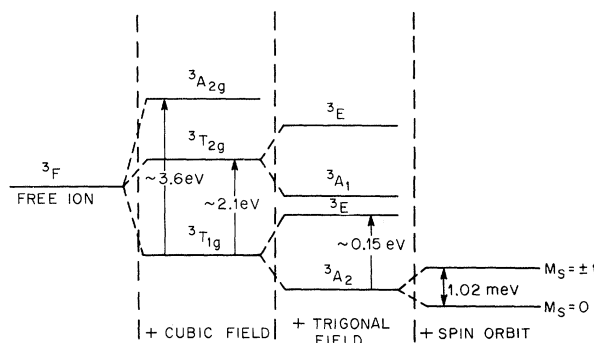


FIG. 11. The effect of various crystalline fields in the energy levels of V^{3+} . The ground-state splitting of 1.02 meV is appropriate for Al_2O_3 .

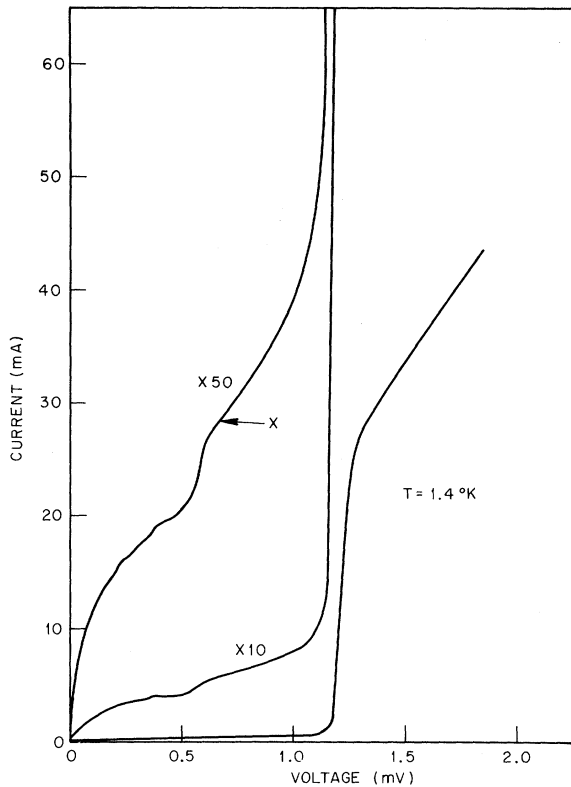


FIG. 12. I - V characteristic of a typical Sn-I-Sn tunnel junction prepared on a Ge:Sb crystal.

the reader is referred to the literature on the subject.⁷⁴ The junctions had typically 10–50-m Ω resistance in the normal state, and all but the highest-quality devices were rejected. Typical resistance ratios R_s/R_n (resistance in superconducting state/resistance in normal state) at biases $V < 2\Delta/e$ ranged from 20 to 50 for useable junctions at 1.4 °K ($T/T_c = 0.37$). By the application of a small (25 G) parallel magnetic field all Josephson effects (dc supercurrent as well as the ac-generated, finite-voltage Fiske modes) were suppressed. If supercurrent behavior persisted out to higher fields, this was an indication that small metallic (superconducting) shorts penetrated the oxide and the net conduction through the barrier consisted of a supercurrent portion in addition to the true tunneling contribution. It was found experimentally that any junctions displaying this shortlike behavior did not detect properly, and they were consequently rejected.

In Fig. 12, we display the I - V characteristics of one of the actual Sn-I-Sn junctions used as a detector in some of this work. This specific junction was a useable detector of average quality. It showed a highly nonlinear characteristic at biases $V < 2\Delta/e$ reflecting thermal excitations and the so-called “mid-gap bump”⁷⁵ at $V = \Delta/e$. For detection,

the device was typically current biased at the point marked \times in Fig. 12 (on the most linear portion of the curve). For most of this work, because of the small magnitude of the signal, the response was linear. The operator of the detector and its sensitivity were discussed in Sec. II and will be reviewed in Sec. IV.

In the fluorescence experiment the superconducting-film generator was insulated from the evaporated constantan heater by a thin (5000-Å) evaporated film of silicon oxide. (The geometry of the experiment is shown in the insert of Fig. 19.) The $\text{Pb}_{0.5}\text{Ti}_{0.5}$ alloy film was prepared by a pellet-flash evaporation technique described previously.⁷⁶ Great care had to be taken, in the preparation of this superconductor-insulator-heater sandwich, to assure that the heater was not shorted through the insulator to the superconductor. This electrical continuity can be a result of inhomogeneities on the surface of the crystal (scratches, etc.), insufficient insulator thickness, or physical damage while attaching the leads to the heater.

The concentration of Sb used in the propagation studies in Ge was 1.8 or $6 \times 10^{15} \text{ cm}^{-3}$. The concentration was determined through resistivity measurements. The samples were rectangular with typical dimensions $\sim 0.4 \times 0.4 \times 1.25 \text{ cm}^3$, the long dimension being in the [111] direction. In all cases the propagation direction was $[1\bar{1}0]$ and a typical flight time over the 0.4-cm distance was $\sim 1 \mu\text{sec}$, the exact value depending upon the polarization of the particular mode. The measurement on the $\text{Al}_2\text{O}_3:\text{V}^{3+}$ was made on a crystal of size $1.5 \times 1.5 \times 1.3 \text{ cm}$ containing $4.5 \times 10^{19} \text{ cm}^{-3} \text{ V}^{3+}$ ions. This concentration was determined optically⁷⁷ by measuring the absorption coefficient of the ${}^1A_1(t^2) - {}^3T_1(t^2)$ transitions of V^{3+} which occur at 20 017 and 21 025 cm^{-1} in σ and π polarizations, respectively, at 77 °K. Far-ir studies on our crystal revealed the presence of a small concentration of V^{4+} (peak absorption coefficient of the $E_{3/2} \rightarrow E_{1/2}$ transition at 28 cm^{-1} was $\approx 0.4 \text{ cm}^{-1}$ at 6 °K). No other impurity absorptions, such as Ti^{3+} which has been detected by other workers⁶⁸ in doped Al_2O_3 , was found in our crystal. The phonons propagating in the c direction were detected by thin-film tunnel junctions of dimensions 1 mm \times 1 mm and the majority of the experiments (except for the T dependence discussed in Sec. IV) were performed at 1.4 °K.

The uniaxial stress was applied using a system similar to that described by Sell and Kane.⁷⁸ The stress was measured by a Kistler 912 quartz force transducer whose generated voltage was amplified by a Keithley model 610B electrometer, the output of the latter was fed directly into the x axis of an XY recorder. Particular care was taken to apply uniform stress over the entire sample as in the early experiments spurious structure resulted

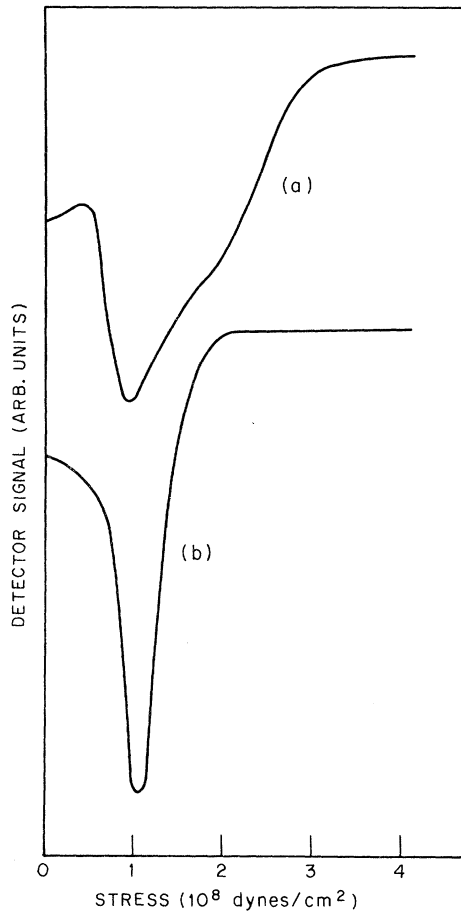


FIG. 13. Change of shape of phonon resonance at 1.20 meV (1.09×10^8 dyn cm^{-2}) with (a) nonuniform stress, (b) uniform stress. The high-energy shoulder in case (a) moves to lower values of stress and merges with the main resonance as the stress is made more uniform.

from inhomogeneous stress. The difference in the resonance absorption line when the stress is not uniform is illustrated in Fig. 13. Here a second well-defined shoulder is evident on the sample where stress is not uniform. The position and strength of this structure varies depending upon the nonuniformity of the stress and was eliminated entirely when maximum care was taken. It was imperative that the (111) faces be flat and parallel to within minutes of arc, and Apiezon J-oil and masking tape were used to reduce remaining inhomogeneities.

The transmitted signal was measured in one of two ways, either by an ac-modulated dc technique which time integrated over the arriving modes, or by a pulsed, time-of-flight method by which the individual polarization modes could be detected and the modal dependence determined. In Fig. 14 we show block diagrams of the two methods used. In the dc method, a constant dc current bias was ap-

plied across the generator junction or heater and a small ac current modulation (500 Hz) superposed. A PAR phase-sensitive detector was then tuned to this frequency at the receiver junction (biased at $eV < 2\Delta$) and the derivative of the total signal detected. This system had the advantage that it was quite sensitive and at relatively low-power levels the signal was still detectable. On the other hand, if high bias and high-power levels were desired, this dc method resulted in an over-all heating of the system, and it was necessary to go the pulsed technique. In this system as is shown in Fig. 14, the generator (junction or heater) was current pulsed with typically a 0.05- μsec -wide pulse, the arriving signal displayed on a scope, signal averaged by a boxcar integrator, and then fed into the y axis of an X-Y recorder.

This pulsed technique had certain advantages and disadvantages. One of the most serious problems with the pulse system is that of impedance matching to 50- Ω cable. Without good matching a certain amount of circuit ringing persisted, in some cases, for a sufficiently long time to mask the arriving signals. It was not possible to increase the resistance of the detecting junction to such a value that the resistance at $V < 2\Delta$ was ~ 50

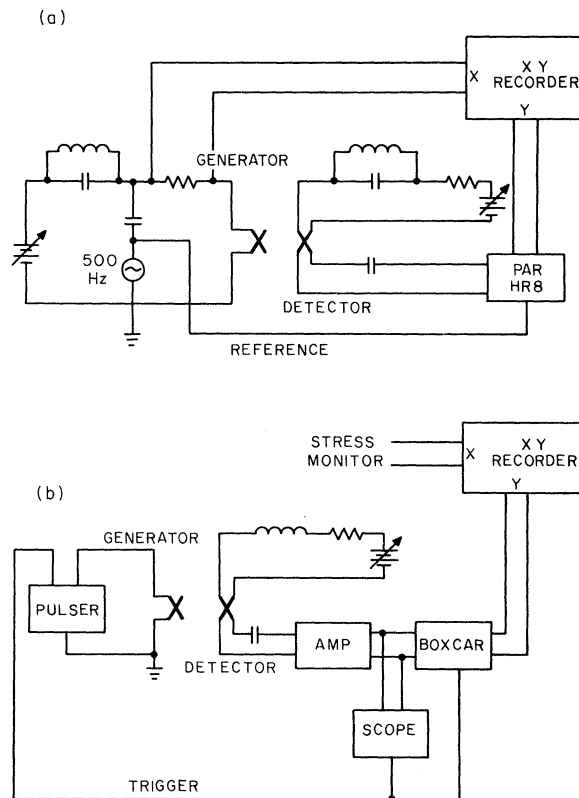


FIG. 14. Block diagram of experimental arrangement. Case (a) dc experiment. Case (b) pulsed experiment.

Ω as the junction response time (the RC time constant for an equivalent resistor and capacitor in parallel) then became too large for submicrosecond detection. For typical tunnel junctions of size 1×1 mm with an oxide of $\sim 10 \text{ \AA}$, the RC time constant at $50 \text{ } \Omega$ becomes of the order of microseconds, making the time resolution impossible. On the other hand, ringing could be minimized by proper grounding of leads and, after some care, was not a serious factor for lower-impedance junctions.

The obvious advantage of the pulsed technique was the ability to inject relatively high levels of power for short periods of time without the entire system heating up. In this way power dependences could be conveniently studied simply by increasing the amplitude of the current or voltage pulse in the generator. The other main advantage of the pulse technique was the ability to discern modal dependence by the time-of-flight separation. This proved invaluable, not only in determining that we were, in fact, seeing phonons propagating and not some other form of energy, but also was absolutely necessary in the $\text{Al}_2\text{O}_3: \text{V}^{3+}$ experiment. Here it was necessary to measure the relative strengths of the transverse and longitudinal transmitted signals to determine whether we were observing the resonance scattering.

For magnetic field tunability, a small superconducting coil coaxial to the sample stick was employed, being capable of supplying ~ 3 kG. In order that the gap parameter Δ be uniform over the thin films, the thicknesses were kept $\lesssim \lambda$ or $\sim 600 \text{ \AA}$. It was found that the detecting tunnel junction also supplied a convenient check for parallelism, the I - V curve in the superconducting state being particularly sensitive to trapped flux. It was found that after careful aligning of the coil with the sample, the H field could be cycled close to (but not above) H_c for the films and could then turned off again with very little or no detectable change in the I - V characteristics. Any perpendicular component of field resulted in trapped flux in the films which was readily detected as a rounding and general decrease in over-all quality of the I - V characteristic. This component caused a spatially dependent gap parameter which was to be avoided.

IV. EXPERIMENTAL RESULTS AND DISCUSSION

In this section, we present the results of the various experiments performed and the implications of these results to our understanding of the basic interactions in the various systems. We first discuss the double-tunnel-junction experiment (tunnel junction both as a generator and detector) and the results of propagation in $\text{Ge}:\text{Sb}$. We then present the heater-superconductor results which confirm that our discussion and calculations in Sec. II are qualitatively correct. The magnetic field

tunability of the system is discussed in a phenomenological way and a practical criterion for choosing the gap edge is presented. In view of this tunability, the results of an experiment designed to observe the resonance absorption of 1.02-meV phonons by the 3A_2 ground state of the V^{3+} impurity level in Al_2O_3 are described. Finally, the power and pulse-width dependence of the propagating phonon beam are discussed and their relation to the relaxation and recombination rates of quasiparticle excitations in superconductors pointed out. These rates are such that a superconductor, where phonon emission is concerned, behaves like a three-level system with some interesting consequences.

A. Double-Junction Experiment

The results of a double-junction experiment (one as an emitter and one as a detector) can be used to derive a picture of what is happening in the generating tunnel junction. We describe here first the results of the dc experiment (using a low-frequency-modulation technique as described in Sec. III).

In Fig. 15 the derivative of the detected signal (s) is plotted as a function of generator bias current $[(ds/dI)_{\text{gen}} \text{ vs } I_{\text{gen}}]$ along with the results of a straightforward calculation assuming the fluorescence model discussed previously. This calculation is performed in the "linear" limit²⁷ where the number of injected quasiparticles is small compared with the number excited thermally. The absolute magnitude is fitted at a bias corresponding to $eV = 6\Delta$. We see that for current biases such that $eV < 4\Delta$, the signal is linearly rising (ds/dI is constant) as the only phonons being detected are those caused by the recombination process. As discussed earlier, the picture is that each tunneling quasiparticle injected into the superconducting film at an energy eV_1 ($eV_1 \leq eV$) relaxes to the gap edge in a time which is very fast compared with the recombination time. This relaxation time is very energy dependent, determined by the electron-phonon coupling strength and the phonon density of states, but is typically 10^{-10} – 10^{-11} sec. In this relaxation process, a single phonon of energy $eV_1 - 2\Delta$ is emitted. (Multiple-phonon processes are much less probable.) For biases $eV < 4\Delta$ this phonon created by relaxation is of energy $\hbar\omega < 2\Delta$, is long lived in the superconductor and escapes into the adjacent dielectric. It is, however, not detected by the detector junction because of its low energy. The remaining particle then stays at the top of the energy gap for a relatively long time (the quasiparticle recombination time is essentially a function of population density, being of the order of 10^{-7} sec), then pairs with another excitation of the required spin and momentum, such that they become a Cooper pair, giving off a phonon of energy $\hbar\omega = 2\Delta$.

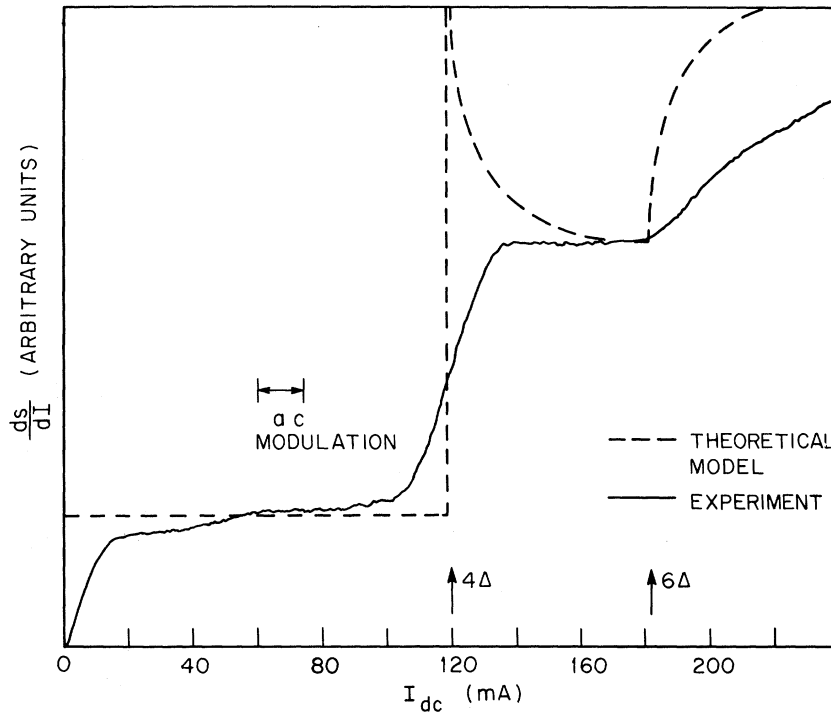


FIG. 15. Experimental and theoretical curves of derivative of detector response as a function of generator current for an Sn-I-Sn tunnel junction. The theoretical curve was calculated assuming a temperature of 0°K and complete reabsorption of phonons of energy $\hbar\omega > 2\Delta$. See text.

Two quasiparticles are thus needed to create one phonon of energy 2Δ . If, however, the bias of the generator junction is increased to such a point that $eV > 4\Delta$ a certain portion of the injected particles (those with $eV_1 \geq 3\Delta$) are capable of relaxation to the edge of the energy gap emitting a phonon $\hbar\omega \geq 2\Delta$ (which can be detected) thus contributing one detectable relaxation phonon and joining with another quasiparticle in the creation of a recombination phonon of 2Δ . For this reason, the level ds/dI above 4Δ should be twice that for biases $< 4\Delta$. The calculation of Fig. 15 predicts a square-root singularity at the rise, reflecting the BCS density of quasiparticle states at the gap edge. Very little of this singularity is seen although the step rise twice that below 4Δ is clearly visible. Some possible reasons for not seeing this singularity will be discussed shortly. In addition, at biases corresponding to $eV \approx 2\Delta$ we consistently observe a small step which at present is not understood. Other investigators^{3, 26, 27} have previously reported structure in this region of a different nature. It is possible that this step is due to the anisotropy of the superconducting energy gap but this possibility has not yet been investigated in detail.

At biases corresponding to $eV > 4\Delta$, according to this picture the relaxation phonon from the highest injected level has an energy $\hbar\omega > 2\Delta$. According to our fluorescence picture, the mean free path for this phonon is very short and at 0°K will tend to break Cooper pairs. This creates two additional quasiparticle excitations, whose energies are de-

termined by the probability factor which is the integrand of the second expression of Eq. (10). At biases corresponding to $eV > 6\Delta$, additional channels for the emission of 2Δ phonons are opened as it becomes energetically possible in some cases for the production of two relaxation phonons of energy 2Δ . This increased signal is reflected in the rise of ds/dI at the corresponding bias (6Δ). In the corresponding calculation of Fig. 15, employing this picture and Eq. (10), we see qualitative agreement with experiment as we see a sharp rise at 4Δ (corresponding to the onset of detection of relaxation phonons) and a further, though lower-order enhancement at 6Δ , corresponding to creation of (multiple) relaxation phonons that can be detected. There are discrepancies between the calculated and observed curves which are not understood as yet. Experimentally a modulating signal of amplitude corresponding to that indicated in the figure was applied; this would tend to broaden out the theoretical curve, but will not explain all the discrepancies. It is possible that these differences are due to the fact that the calculations are performed ignoring $k_B T$ smearing. This assumption is not true as the experiments were performed at 1.4°K ($T/T_c \approx 0.37$) and the very fact that we are injecting excitations via tunneling guarantees that many of the levels at the gap edge are occupied. Both of these effects would tend to eliminate the calculated singularities and produce a result approaching that observed experimentally.

In a similar experiment²⁷ using Pb junctions in-

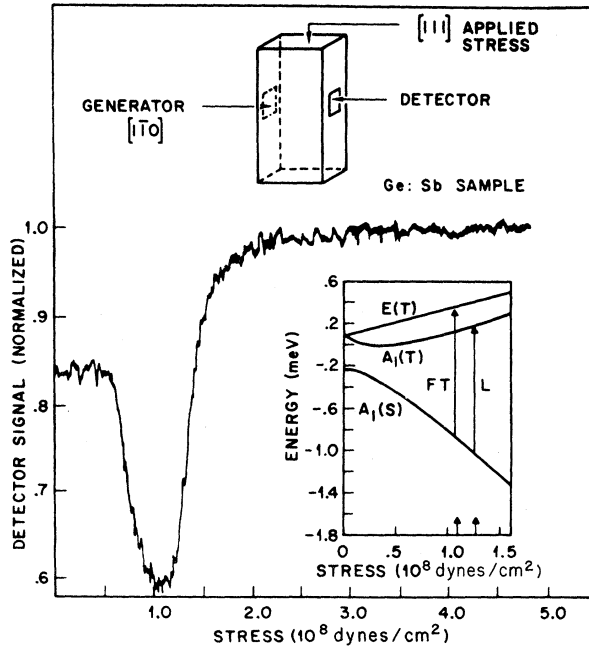


FIG. 16. Tracing of detector signal as a function of stress in the dc experiment. Sn-I-Sn tunnel junction generator and detector. Phonon-propagation direction is $[1\bar{1}0]$. Applied compressive stress is along $[111]$.

stead of Sn, results more similar to those calculated in Fig. 15 were obtained. This could be due to the fact that, as lead has a substantially higher critical temperature (7.2°K as opposed to 2.8°K) and the energy gap is correspondingly larger ($2\Delta = 2.80\text{ meV}$ compared with 1.2 meV), these experiments were performed at a much lower effective temperature. Here, the assumption of empty states above the gap edge and $T = 0^\circ\text{K}$ is more closely approximated. (See note added in manuscript.)

A similar calculation has been performed by Kinder, Laszemann, and Eisenmenger²⁶ in which the density of relaxation phonons was modulated by the lifetime of the excited state in the BCS approximation, as calculated by Tewordt. Their calculation does not show as strong a singularity at 4Δ . This may be due to the finite lifetime effects.

With these restrictions in mind, the comparison of experimental results with calculations certainly indicates that phonons with energies $\hbar\omega > 2\Delta$ are extremely short lived in a superconductor and cause additional pair breaking. This is confirmed by the further enhancement of the signal at 6Δ corresponding to multiple processes. In the absence of phonon reabsorption, there would be no additional structure above 4Δ . The over-all qualitative agreement of the calculation with experiment indicates that the gross features of our model must be correct.

Utilizing the stress-dependent properties of Sb-donor levels in Ge and a tin-tunnel-junction detector as outlined in Sec. II, the energy spectrum of phonons emitted from a tunnel junction has been investigated. Biasing the generator junction at $2\Delta < eV < 4\Delta$ (where only recombination phonons of energy $\hbar\omega = 2\Delta$ will be detected) a plot of detector signal as a function of $[111]$ uniaxial stress was obtained as shown in Fig. 16. Again we emphasize that nonuniform stress resulted in plots similar to that shown in Fig. 13 where a well-defined but spurious shoulder was resolved. In Fig. 16 we see a clearly resolved absorption at $1.09 \times 10^8\text{ dyn cm}^{-2}$ corresponding to a stress splitting of 2Δ and a FT absorption from $A_1(S)$ to $E(T)$. From our previous discussion we know that for propagation in $[1\bar{1}0]$ the selection rules allow only an L -mode coupling from $A_1(S)$ to $A_1(T)$ and FT-mode coupling from $A_1(S)$ to $E(T)$. For $E_u = 16\text{ eV}$ (that obtained from ir absorption) this resonance corresponds to the FT coupling, and we see no indication of the L absorption expected at higher stress. We expect to see both absorptions as a doublet in this dc experiment. In fact, if expressions (21) or (22) are correct, then from these terms, illustrated in Figs. 8 and 10, we would expect the L absorption from $A_1(S)$ to $A_1(T)$ to be comparable or an order of magnitude stronger than the FT scattering. Physically this is simply due to the fact that for an energy of 1.2 meV the longitudinal wavelength is approximately 1.5 times that of the transverse mode, and since the Hasegawa scattering term cuts off as a large power of q a large difference results. No L absorption was seen, however, and the reason for this will be discussed shortly in the description of the pulsed experiment.

The linewidth of the absorption was not an indication of the inherent linewidth of the 2Δ monochromatic phonons. It was limited by the uniformity of the stress applied and varied from experiment to experiment, the minimum yet achieved being of the order of 20%. For low levels of excitation it is believed that the true linewidth is smaller than this value, of the order of the energy-gap anisotropy, i.e., $\approx 5\text{--}10\%$. The line shape (both strength and width) was independent of the dc bias on the generator (for biases $> 4\Delta$) confirming our previously stated belief that all the phonons injected into the Ge were of an energy $\leq 2\Delta$. If higher-energy phonons were generated, as one might expect in the relaxation process, they would appear as absorptions at larger stress in these plots. That this was not the case leads us to the conclusion that the high-energy relaxation phonons are short lived and cause pair breaking in the superconductor, degenerating to a large number of lower-frequency phonons. The dc powers generated in this experiment were typically of the order of a few milliwatts before heating ef-

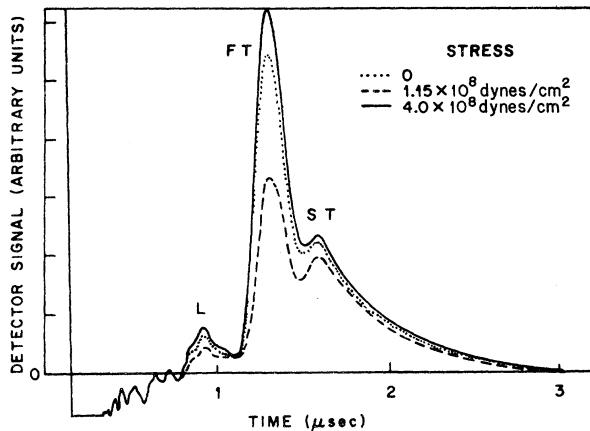


FIG. 17. Tracing of boxcar output as a function of time for three values of stress. Pulsed-double-junction experiment. Peak generator current 1.5 A. Pulse duration 0.05 μsec .

facts became significant. This does not mean that all of this power was in the 2Δ phonons detected at the other junction. As can be seen from our calculations of Fig. 2, a substantial portion of the power is composed of phonons of energy $< 2\Delta$ which are not detected.

In order to determine the modal dependence of the absorption, a pulsed, time-of-flight experiment was performed in which the modes were velocity separated as described in Sec. III. A typical arriving signal as a function of time is illustrated in Fig. 17 where we see clearly the resolution of the L , FT, and ST modes for the $[1\bar{1}0]$ direction. The sound velocities, measured in this experiment, were in good agreement with those measured previously using conventional methods. In this figure we also see the reason why the expected $A_1(S) \rightarrow A_1(S)$ resonance absorption of the L mode was not also observed in the dc experiment. The intensity of the FT mode is much stronger than the L mode, hence in a time-integrated experiment the L mode contributes very little to the total signal. This dominance of the FT mode over the L and ST modes is due to elastic anisotropy in Ge, causing focusing of this mode into the beam direction for the $[1\bar{1}0]$ propagation. In an anisotropic medium, the direction of energy flow is not in general the same as that of the \vec{q} vector.¹⁸ This has the effect of enhancing the energy flow for some modes in some directions and defocusing others. From these considerations, it is in fact expected that, as observed, for propagation in the $[1\bar{1}0]$ direction the FT mode would dominate. This was quantitatively calculated to yield values for the intensity ratio of 8 for I_{FT}/I_L and 0.8 for I_{ST}/I_L in good agreement with that observed in our experimental geometry. Intensity variations due to the modal

dependence of the electron-phonon coupling in the superconductor are expected to be small as discussed in Sec. II. This is confirmed by our results in Al_2O_3 where elastic anisotropy is small.

To observe the modal dependence, the L - and FT-peak strengths were monitored as a function of stress. The results of that study are shown in Fig. 18 where the signal strength is presented in normalized units. Here it is clear that the splitting between the FT and L mode obeys, as expected, the selection rules outlined in Fig. 6. The slight variation in the ST peak in Fig. 17 is believed due to the changes in the overlapping tail of the much stronger FT mode and probably obeys the selection rules forbidding coupling to the Sb donors. It should also be noted that, contrary to the predictions of Figs. 7 and 8, the relative absorptions are approximately equal for the two modes. The q -cutoff term predicts an order-of-magnitude difference in their scattering which is not seen. This point will be commented upon later. Finally, for pulse powers up to 100 mW (biases up to 150Δ) no visible change, either in line shape or intensity, was observed in these absorption peaks. This observation is consistent with the previous dc observation that the line shape was invariant to the dc bias. Again, the linewidth of these absorptions should not be interpreted either as the inherent linewidth of the generated phonons or the lifetime broadened width of the Sb hydrogeniclike levels in Ge. It is most probably dominated by broadening due to nonuniform stress, as from experiment to experiment it varies from 20–33%.

As was suggested previously, the peak-absorption positions correspond to resonant absorptions of $A_1(S) \rightarrow A_1(T)$ for L and $A_1(S) \rightarrow E(T)$ for FT. Assuming phonon energies $\hbar\omega = 2\Delta = 1.2$ meV, it is found that a best fit to Eqs. (13) and (14) are obtained from the results if E_u is assumed to be 16.0 ± 0.5 eV. This is in good agreement with Reuszer and Fisher,⁶² who studied these levels by infrared sideband absorption, and is felt to be a direct confirmation of these earlier results.

In addition to the resonance scattering discussed above, there appears to be an off-resonance scattering as reflected in the shift of the baseline of Figs. 16 and 18. Possible origins of this will be discussed later.

B. Phonon Fluorescence

An experiment, designed to test the ideas outlined in Sec. II C and Figs. 2–4, was performed in which a heat pulse from an evaporated constantan film was shone into a thin (600-Å) tin film. To discern the spectrum emitted from such a device, the Ge:Sb system was again used as a spectrometer in conjunction with a tunnel detector on the opposite face. Again propagation was in the $[1\bar{1}0]$ direction

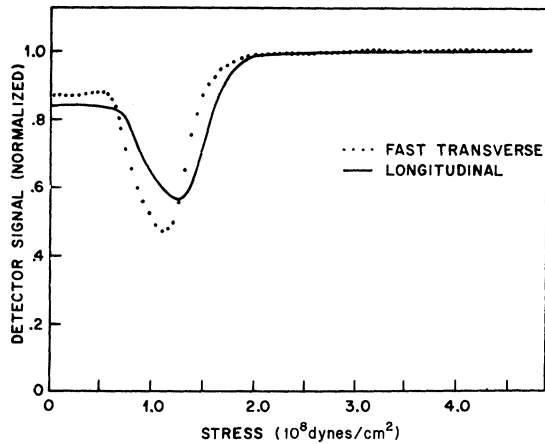


FIG. 18. Tracing of peak intensities as a function of stress of longitudinal and fast transverse modes. Double-junction experiment.

and the uniaxial stress was applied in the $[111]$ direction. The detector junction was sensitive only to phonons of energies $\hbar\omega \geq 2\Delta$. The experiment was performed using the pulsed, time-of-flight-measurement method. To discern whether the emitted spectrum was of the type anticipated in Fig. 2 or simply of the more conventional heat pulse (blackbody distribution), the peak strength of the FT mode as a function of uniaxial stress was measured and the results are illustrated in Fig. 19. The absorption curve is qualitatively similar to that of Fig. 18 for the double-junction experiment.

Because the detector is sensitive only to phonons of energy $\geq 2\Delta$ this plot tells us that there is a sharp cutoff at 2Δ in the spectrum emitted from the heater superconductor combination. The results are consistent with the calculated spectrum of Fig. 2 but from this experiment there is no way of discerning the relative proportion of phonons of energy equal to 2Δ to those of lesser energy.

It is also worth noting that this result experimentally confirms the previous conjecture that the mean free path of high-energy phonons ($\hbar\omega \geq 2\Delta$) is of the order of or less than the thickness of the film used in this experiment ($\sim 600 \text{ \AA}$). At these higher energies and q vectors, umklapp processes become allowed. In fact, in the extreme case of the free-electron approximation, it turns out that for Sn we estimate U processes are about 10 times more likely than N processes and the estimated mean free path is very short. Because details of the Fermi surface are very important in any estimate of the strength of U processes for a real system, the calculation is very difficult but these experimental results clearly indicate that the absorption is comparable to our estimates at these high frequencies.

It was desirable for two reasons to repeat the above experiment using as a generator a superconductor whose energy gap 2Δ was greater than that of Sn (1.2 meV). Pb ($2\Delta = 2.8 \text{ meV}$) was the obvious choice but because power considerations demanded an unreasonably high effective heat-pulse temperature to obtain a reasonable signal (see Fig. 2) the

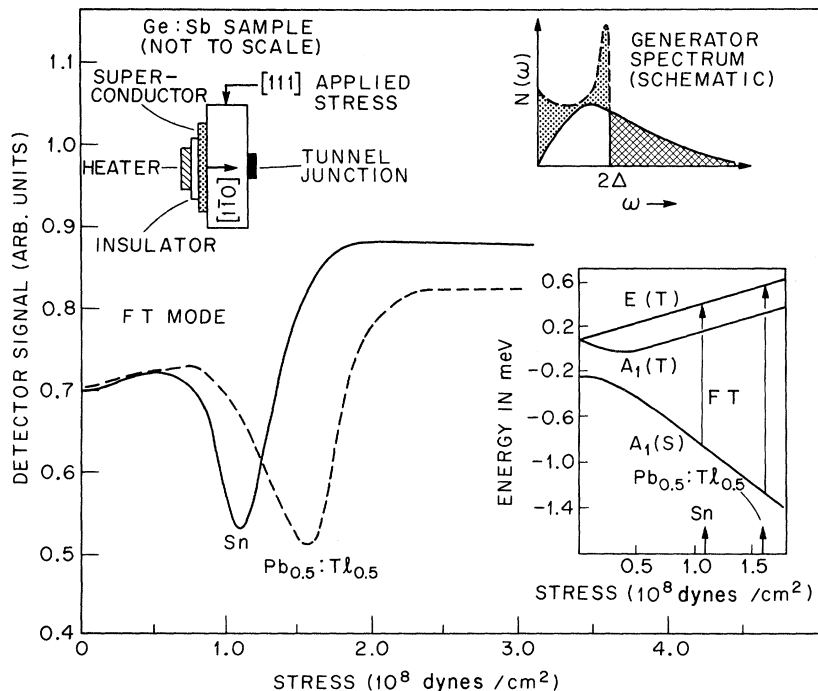


FIG. 19. Tracing of peak intensity of FT mode, propagating along $[1\bar{1}0]$ as a function of stress for Sn and $\text{Pb}_{0.5}\text{Tl}_{0.5}$ generators. Phonon-fluorescence experiment. Power density 0.22 W/cm^2 ; pulse width 0.05 \mu sec .

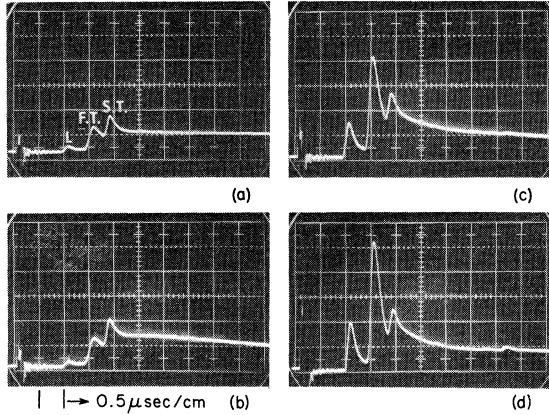


FIG. 20. Photographs of ballistic heat pulses in Ge:Sb. $N_d = 6 \times 10^{15} \text{ cm}^{-3}$. Time scale $0.5 \mu\text{sec}/\text{large division}$. Case (a) 0 stress. (b) $1.3 \times 10^8 \text{ dyn cm}^{-2}$. (c) $2.5 \times 10^8 \text{ dyn cm}^{-2}$. (d) $4.5 \times 10^8 \text{ dyn cm}^{-2}$. Path length 4.8 mm. Propagation direction $[\bar{1}\bar{1}0]$. Stress direction $[111]$. Pulse power 0.4 W/mm^2 .

alloy $\text{Pb}_{0.5}\text{Tl}_{0.5}$ was selected instead. 2Δ for this alloy, as measured by a conventional superconducting tunneling experiment⁷⁹ was 1.7 meV. The two reasons for choosing a superconductor with a gap larger than that of Sn were as follows.

(i) By using a Sn tunnel junction as a detector we were sensitive to phonons of energies $\geq 1.2 \text{ meV}$ while $2\Delta_{\text{alloy}} = 1.7 \text{ meV}$. Hence, we could evaluate in a more quantitative fashion the strength of the peak in the spectrum at $2\Delta_{\text{alloy}}$ relative to the background lower-energy modes ($1.2 < \hbar\omega < 1.7 \text{ meV}$). In this way we could determine whether our calculations of Fig. 2 were qualitatively correct.

(ii) From Eq. (21), we see a very strong dependence of the scattering rate on wave vector \vec{q} . [$1/\tau$ varies as $F^4(q)$. F varies as $1/q^4$ at large values of q .] Hence, as is seen in Fig. 8, there is a strong cutoff in the scattering rate predicted by this expression at higher energy. In view of this strong dependence on energy it was important to demonstrate that phonons of higher energy than those of $2\Delta_{\text{Sn}}$ can also experience this resonance absorption with a magnitude of the absorption coefficient similar to that observed in Sn. Otherwise it could be argued that the sharp cutoff on the high side of the resonant peak was due to this strong q -dependent cutoff of the scattering.

The signal strength of the arriving FT mode at 1.2 meV and greater, as a function of $[111]$ uniaxial stress, is displayed as the dashed line in Fig. 19. Two things are worthy of note. First, it is clear that with the same concentration of Sb in Ge as studied previously with a Sn generator, the absorption strength is of the same magnitude. This observation confirms that higher-frequency phonons are also scattered by the level splitting and the q cutoff

expected is not as severe as predicted in Eq. (21). Second, it is shown in these data that there is in fact a strong peak in the phonon distribution at 2Δ relative to those energies $< 2\Delta$. This experiment qualitatively confirms our calculations of Fig. 2 where we predict a substantial peak at 2Δ . It should be noted that there is a slight asymmetry in this resonance peak, showing stronger absorption on the lower-energy side. It is possible that this asymmetry is a reflection of the signal expected at the lower side of the distribution.

In order to reconfirm that the observed resonance peak was a result of down conversion of high-frequency phonons, the experiment was repeated with Ge:Sb and a bolometer detector but with simply a constantan film as a generator. It has been shown previously that this type of generator emits a phonon distribution characteristic of a blackbody radiator with an effective temperature T_h greater than the ambient temperature T_a of the bath. From (4) we know that, for $T_h \gg T_a$,

$$V_i^2/R = \sigma T_h^4,$$

i. e., the characteristic temperature of the distribution varies as the square root of the voltage applied across the heater. Consequently, the peak in the distribution of emitted phonons must move as the voltage is increased, while for the spectrum emitted from a superconductor, the peak remains constant, assuming the *real* temperature shifts are not significant enough to vary the gap energy.

In Fig. 20 we show typical ballistic heat pulses in a Ge crystal containing $6 \times 10^{15} \text{ cm}^{-3} \text{ Sb}$, for four values of uniaxial stress and at a generator power density of 0.4 W/mm^2 , a value close to that used in our fluorescence experiment. The higher-Sb concentration was used in this experiment since the broad resonance absorption with heat pulses was barely discernible in the lower-concentration crystal. From Fig. 20 the strong variation in intensity

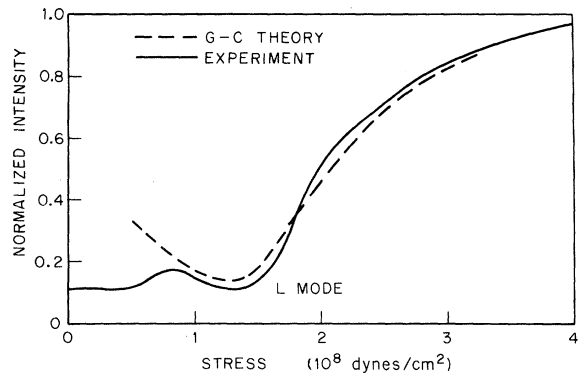


FIG. 21. Normalized intensity of longitudinal heat pulse as a function of stress. Dashed line calculated according to theory of Griffin and Carruthers. See text.

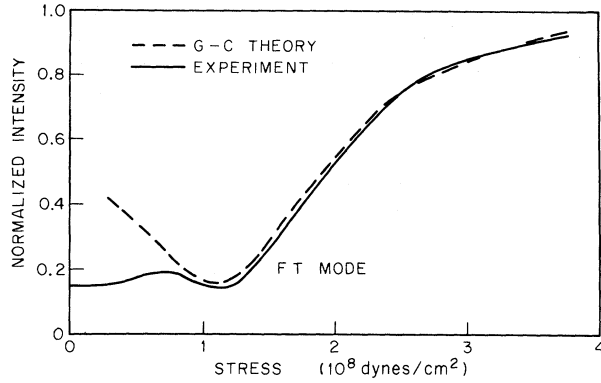


FIG. 22. Normalized intensity of fast-transverse heat pulse along $[1\bar{1}0]$ as a function $[111]$ stress. Dashed line calculated according to Griffin-Carruthers theory. See text.

of the L and FT modes relative to the ST mode is evident, and this serves to reconfirm the selection rules derived earlier.

Figures 21 and 22 show a quantitative plot of the intensity of the L and FT modes as a function of stress. The chief difference between these curves and the fluorescence experiment is the weakness of the resonance and the long high-energy tail characteristic of a heat pulse. The theoretical curves were calculated using the Griffin-Carruthers (GC) expression (22) with $\gamma=0$ and Eq. (5) for the attenuation of the ballistic heat pulses. Excellent agreement between theory and experiment is obtained for a value of $T_h = 3.7^\circ\text{K}$ for a power density of 0.4 W/mm^2 . The theoretical curves were calculated only for values of stress greater than $0.5 \times 10^8\text{ dyn cm}^{-2}$ since for lower values the splitting changes relatively little, due to the quadratic variation with stress of the A_1 states. Very little variation in the absorption is expected for lower values of stress. Attempts to fit the observed curves with the Keyes scattering term were totally unsuccessful because of the almost identical strengths of the L and FT scatterings observed experimentally. The Keyes term alone predicts more than an order of magnitude greater L absorption than FT mode absorption. In addition it cannot explain the observed resonance.

In Table I we summarize the heat-pulse results for four values of power. It is clear that the heat-pulse temperature determined by the Ge:Sb spectrometer is very close to that calculated according to the blackbody-radiation formula assuming perfect coupling of the thermal energy to the Ge crystal. This perfect-coupling formula has the form

$$P/A = \bar{v}^s \rho \int_{T_s}^{T_h} C_v dT = \frac{1}{4} \bar{v}^s \rho \alpha (T_h^4 - T_s^4), \quad (26)$$

where $C_v = \alpha T^3$ is the specific heat of the crystal

under study, ρ its density, and \bar{v}^s is the average sound velocity which is close to the transverse sound velocity.

In the context of the perfect-coupling model the chief experimental error is the heat loss due to the immersion of the sample in liquid helium. This is, however, a moot point since this is expected to cause an error of at most the fourth root of 2 in the value of T_h .

In summary, the results of the heat-pulse experiment into our spectrometer do, in fact, clearly show that the broad thermal distribution from a heat pulse shifts with increasing voltage across the heater in quantitative agreement with our ideas. No sharp resonance-absorption line as seen in the superconductor experiments was observed.

An interesting consequence of this study of resonance absorption by Sb levels in Ge is the lack of agreement with the concept of a strong q -dependent cutoff of the scattering when the phonon wavelength becomes comparable to the diameter of the hydrogeniclike wave functions of the Sb-donor levels. Experimentally, we find that the L - and T -mode scattering are comparable (in violation of this model). Expression (21) is based on a perturbative calculation from a static-interaction point of view and is expected to apply only when the phonon energy is small compared to the stress-induced level splitting. In this work we are looking precisely at the region where the static theory is expected to break down and the calculations of Griffin and Carruthers are more relevant. We see, in agreement with the resonance model the polarization dependence of the resonance peaks are comparable in magnitude (Figs. 18 and 20).

Theoretically, the precise value of these intensities depends critically on the choice of linewidth γ and its stress-splitting dependence. The ω dependence of the absorption strength can be explained through a suitable choice of the stress-splitting dependence of the linewidth. This choice of linewidth of course would depend upon whether the q -cutoff term is included.

This work then suggests that in this energy range the dominant mechanism for scattering of phonons by the Sb impurities is via the resonant-fluores-

TABLE I. Heat-pulse temperature (T_h) for values of power into Ge:Sb. $T_h(\text{expt})$ were obtained from best fits of the data to GC theory. $T_h(\text{calc})$ were obtained from Eq. (26) and known C_v of Ge.

P/A (W/mm ²)	$T_h(\text{expt})$	$T_h(\text{calc})$ (°K)
0.1	2.7	2.6
0.28	3.1	3.3
0.40	3.8	3.7
1.03	4.4	4.6

cence mechanism. From our data we are not in a position to estimate an accurate value of γ , the effective linewidth of the absorption due to finite lifetime effects. We can, however, from the relative absorption at the peak of the resonance curve at 2Δ , determine the appropriate mean free path of phonons of this energy; relate that to the calculations of Eq. (22) and determine that a realistic value for γ is of the order of a few percent.

We now turn briefly to the shift in the baseline as observed in Figs. 18 and 19. We consider three possible explanations for this shift. (a) This increase in signal at large values of stress could be the result of the $F^4(q)$ cutoff factor. However, this appears unlikely because the magnitude of the step is comparable for the L and FT modes and it appears to move with the resonance as one increases the phonon energy. (b) Alternatively, this could arise from inelastic scattering terms involving off-resonance transitions from the singlet to the triplet. Pure inelastic scattering ($\hbar\omega \gg 4\Delta_c$) at 0°K yields a mean free path of ~ 10 cm from the expressions of Suzuki and Mikoshiba.⁸⁰ This value may be considerably shorter if one takes into account inelastic scattering near resonance ($\hbar\omega \approx 4\Delta_c$) and also the possibility of thermally assisted absorption. A quantitative determination of this effect is not possible due to the uncertainty in the value of the linewidth. (c) It is worth noting that the heat-pulse experiments (Figs. 21 and 22) show a qualitatively similar baseline shift with a very broad resonance. It is possible that this similarity indicates that the superconducting generators have a

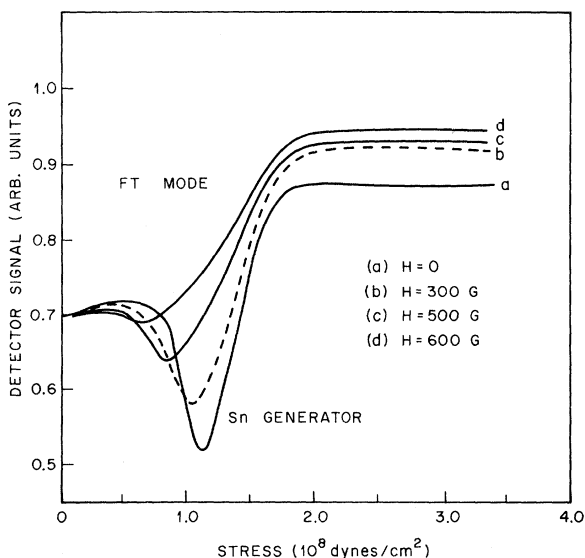


FIG. 23. Intensity of the FT mode for four different values of magnetic field applied parallel to the plane of Sn generator film. Phonon-fluorescence experiment.

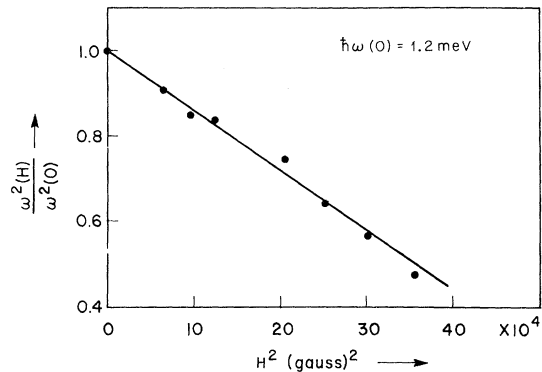


FIG. 24. Plot of the square of resonance frequency $\omega(H)$ as a function of square of applied magnetic field H .

large spike at 2Δ riding on a weak heat-pulse background. The frequency selectivity of the tunnel-junction detector compared to the bolometer complicates this interpretation.

C. Magnetic Field Tunability

As was discussed in Sec. IID and shown previously,⁴⁴ if the superconducting films are sufficiently thin on the scale of the penetration depth λ , the gap parameter is not drastically spatially dependent (Δ is approximately constant throughout the film) and varies monotonically from its maximum value to zero with increasing field, undergoing a second-order transition to the normal state at the critical field [see Eq. (12)]. In Fig. 23 we show a series of absorption curves for a heater/tin-film/Ge/tin-tunnel junction detector system for various applied H fields parallel to the films. Clearly, the peak of the resonance absorption is shifted monotonically to lower energy with higher magnetic field. There is also a decrease in the absorption peak corresponding to this decrease in position. A fit of this peak position (assuming this to be equal to the energy gap 2Δ) to Eq. (12) is shown in Fig. 24 where we indeed see that over the range of tunability good agreement with the straightforward Ginsburg-Landau theory results. For thicker films we have found very little tunability as the gap discontinuously drops to zero at a field approaching the bulk critical field H_{cB} . In addition, the theoretical density of excitations in the presence of a magnetic field deviates from that of the familiar BCS form, and the tunneling I - V characteristics reflect this effect. One cannot interpret the data in the usual BCS fashion. As is shown in Fig. 5, the density of excitations broadens,^{51,52} and the square-root singularity disappears. The gap, however, still displays a sharp edge both theoretically and experimentally and is a monotonic function of applied field.

For purposes of identification of the energy gap

from the I - V characteristics of the tunnel-junction detector, we present here a practical criterion which correlates well with the position of the absorption peak. It is found that the construction described by McMillan and Rowell⁸¹ to determine the energy gap 2Δ in a superconductor-insulator-superconductor tunnel junction can be applied to this system with good results. By extrapolating the almost linear region above 2Δ , and the region below 2Δ and determining the position where the current is halfway between these two extrapolated lines, a good correlation with the peak of the resonance curve is achieved. We see no theoretical justification for such a procedure but the results suggest that this is a sufficiently accurate method for determining an "effective energy gap" at which the peak in the spectrum of emitted phonons occurs.

There are three possible reasons for the decrease in the strength of the absorption peak as a function of magnetic field and all probably play an important part in the final result. First, as was discussed above, the density of excitations in the superconductor is no longer of the BCS shape with the square-root singularity at the gap edge. This modification invalidates somewhat the calculations performed in Sec. II and illustrated in Fig. 2. This effect could tend to broaden the distribution around the peak and put more weight into the lower-energy modes (see Fig. 5) thus decreasing the peak strength. Second, the phonon-defect interaction in

Ge is expected to vary with a high-power energy [see Eq. (22) where $1/\tau$ varies as ω^4]. Inelastic scattering, on the other hand, varies much more slowly with ω . Hence, from these considerations, one would expect the lower-energy resonance absorptions to be substantially weaker. Third, as we are changing 2Δ to lower values, the ratio $2\Delta/k_B T$ becomes smaller, thus increasing the number of thermally excited quasiparticles. As will be shown shortly, this change in the excited quasiparticle density has a profound effect on the emitted spectrum.

The decrease in peak strength is most likely a result of a combination of all three effects and so it is not clear that the limit of tunability of the emitted phonons is $\Delta < \hbar\omega < 2\Delta$. We can only say that using this Ge:Sb spectrometer at 1.4°K we can discern tunability over this energy range.

Using this tunability feature, we have observed, in a direct fashion, the splitting of the 3A_2 ground state of V^{3+} in Al_2O_3 . As outlined in Sec. II E and illustrated in Fig. 11, it is possible to study this level due to the fact that the selection rules allow a coupling to the T modes but not the L modes. Hence by studying the ratio of T and L peaks as a function of emitted phonon energy, we can observe a resonance absorption due to this selective coupling.

Phonons were generated by a constantan-heater-Sn-film arrangement, propagated in the c direction of the Al_2O_3 , and detected by a conventional tunnel junction. Pulse powers were typically of the order of a watt, with pulse widths usually less than 0.1 μ sec except when pulse-width dependences were studied. Good clean L and T pulses were obtained as shown in Fig. 25, with very little ringing, a result of the relatively large path length (1.3 cm) and consequent long delay time between generating pulse and arriving signal. This good signal allowed accurate measurement of the peak strengths and the relative peak heights of the two modes. The pulse marked W is believed to be due to side-wall scattered phonons.

The quantitative results of this experiment are shown in Fig. 26. Here we have plotted the ratio of peak strengths as a function of tuned phonon energy and we see a strong absorption peak centered at 1.02 ± 0.01 meV, exactly where expected. We see that at this concentration (4.5×10^{19} cm⁻³) the absorption peak is approximately 25% of the total signal, and again the linewidth is typically of the order of 20%. From the magnitude of the absorption shown in Fig. 26 and Eq. (25) one can get an estimate for the magnetoelastic coefficient $|G_{44}|^2$. We find a value of 10^{-15} erg (~ 10 cm⁻¹) for $|G_{44}|$. This appears to be the right order of magnitude for this coefficient.

The energy gap of a superconductor varies also

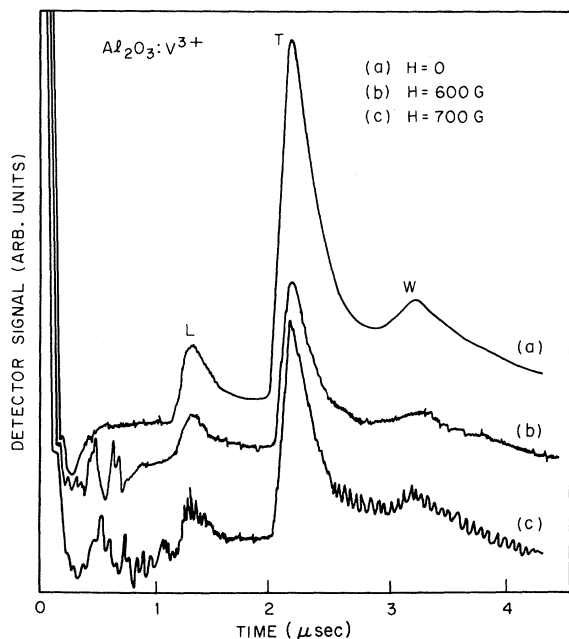


FIG. 25. Ballistic pulses in $Al_2O_3:V^{3+}$ for three values of magnetic field. Propagation direction c axis. Path length 1.3 cm. Phonon-fluorescence experiment. Sn generator. Sn tunnel-junction detector.

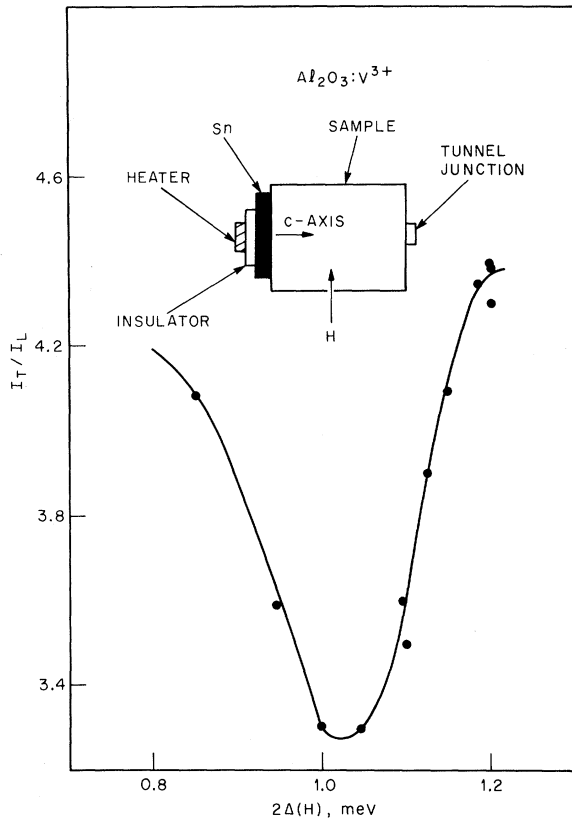


FIG. 26. Ratio of intensity of transverse to longitudinal pulse in $\text{Al}_2\text{O}_3:\text{V}^{3+}$ as a function of energy gap of Sn film. Energy gap determined according to procedure described in text.

with temperature in a monotonic fashion from zero at T_c to its full value at $T=0$. It turns out that the gap varies as⁸²

$$\Delta(T) = \frac{2}{1.14} k_B T_c e^{F(\Delta/k_B T)},$$

where F is a function of the ratio $\Delta/k_B T$. This $\Delta(T)/\Delta(0)$ vs T/T_c dependence is plotted as an insert in Fig. 27 where we see for easily obtainable temperatures one can tune the gap completely to zero. This tunability was utilized on the $\text{Al}_2\text{O}_3:\text{V}^{3+}$ system where, it was hoped, that by temperature tuning the gap one could observe the same absorption level seen in the magnetic field tuned case. The gap was independently measured by plotting the I - V characteristic of the detector junction and the temperature was monitored by the helium vapor pressure.

The unsuccessful results of this experiment are shown in Fig. 27 where we show the arriving pulse as a function of time for various temperatures. It becomes immediately clear that, except for the lowest reduced temperatures, the arriving signal is dominated by a large diffusivelike tail which de-

creases exponentially with decreasing temperature. From these data it is very difficult to extract the ratios of T to L signal. This tail we attribute to the existence of thermally excited quasiparticles in the generating and detecting superconducting films. The population density varies exponentially with temperature; the activation energy being the superconducting energy gap. These quasiparticles have a continuous excitation spectrum over which they can scatter phonons. Consequently, the mean free path for phonons (of all energies) decreases as a result of these new scattering processes and a phonon of energy $\geq 2\Delta$ is not necessarily compelled to pair break. From Fig. 1, it is clear that it can with comparable probability excite an already existing quasiparticle to a higher level. This will not create new excitations which, in the generation process would guarantee a phonon of energy 2Δ , or in the detection phase a subsequent voltage pulse. Consequently, a phonon beam incident upon a superconductor with a finite density of quasiparticle excitations will undergo a subsequent thermalization process. This argument applies both to the generator and detector in our situation, and the net result is a long diffusionlike tail. In the interpretation of the $T=0^\circ\text{K}$ case that we have presented previously, thermodynamic equilibrium is not necessarily reached. This observed temperature dependence cannot be due to scattering processes in the Al_2O_3 crystal as heat pulses at similar power densities propagate with very little attenuation.

From these results, we conclude that it is necessary to perform these experiments at as low a temperature as possible to reduce the number of

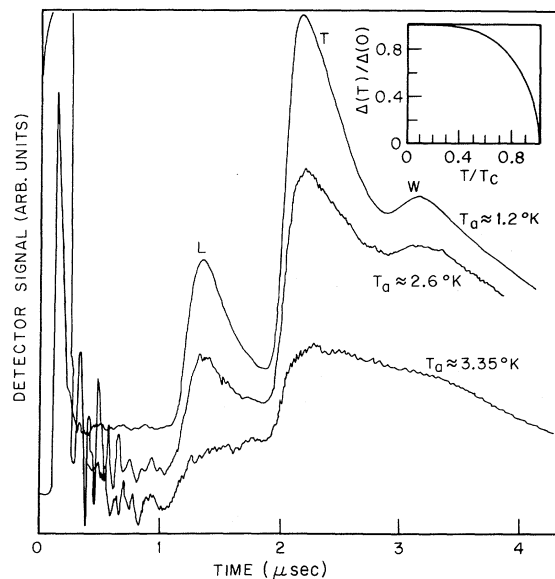


FIG. 27. Temperature dependence of ballistic pulses in $\text{Al}_2\text{O}_3:\text{V}^{3+}$. Phonon-fluorescence experiment.

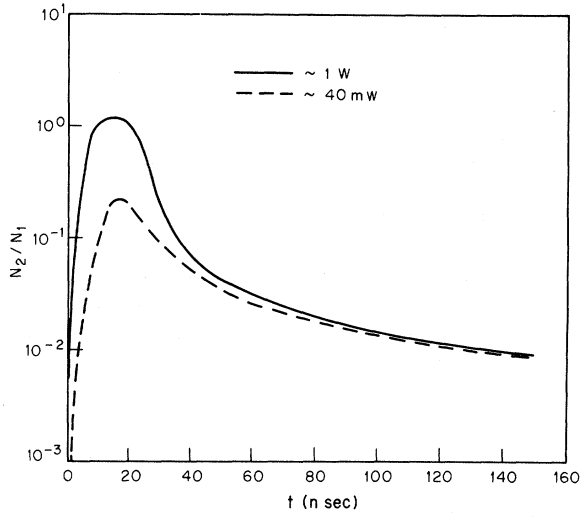


FIG. 28. Theoretical calculation of population ratio of quasiparticles at gap edge to those paired at the Fermi level for different values of pulse power as a function of time. For choice of parameters see text.

thermally excited quasiparticles. If this number becomes significant, other scattering processes will result and our relatively simple 0°K interpretation no longer holds.

D. Power Dependence

The obvious analogy between the model presented here and the familiar three-level optical-laser system leads one to speculate as to whether a population inversion is possible. A phonon incident upon a superconductor ($\hbar\omega > 2\Delta$) will cause pair breaking from the ground state (level one) resulting in excitations in the quasicontinuum of states above the gap edge (level three). These excitations will then decay to the top of the energy gap (level two). Both of these processes are extremely fast ($< 10^{-10}$ sec) and can be assumed to respond immediately on the time scale of the pulses applied in this work (10–100 nsec). The recombination lifetime, on the other hand is typically of the order of or longer than these pulse times. Unlike the optical analogy this lifetime τ_R is inversely dependent upon the population density of this level (N_2).

With these considerations in mind, one can easily write down the rate equations for this system, assuming the transition 3 → 1 is not allowed and 1 → 3 → 2 instantaneously follows the externally applied pulse. We consider a tunnel-junction configuration, and the rate equations for levels one and two become

$$\frac{dN_2}{dt} = \alpha I + 2N_{PB}(\alpha I) - \frac{N_2}{\tau_R},$$

$$\frac{dN_1}{dt} = \frac{N_2}{\tau_R} - 2N_{PB}(\alpha I) - \alpha I.$$

Here, the injected current αI is in units of electrons/sec cm³, and N_{PB} is the nonlinear factor from pair breaking due to high-energy excitations as calculated in Fig. 15. We will assume τ_R varies as $1/N_2$, and τ_R at $T = T_c$ is $\sim 10^{-8}$ sec. For a triangular current pulse of 30-nsec duration, a 10-mΩ junction consisting of films 1000 Å thick, and assuming the density of states at E_F for Sn to be 0.238 state/eV atom, these equations were solved iteratively for $T = 0^\circ\text{K}$ boundary conditions. The calculated ratio N_2/N_1 for two different peak-power levels is shown in Fig. 28 where we see, as expected, a rise in the ratio during the application of the pulse until N_2 becomes comparable to N_1 . After the turnoff of the pulse, we see the expected decay, the decay length of which is population dependent. In fact, we see for reasonably modest pulse powers (≈ 1 W) we have determined that the population will invert ($N_2/N_1 > 1$).

There are, of course, many important aspects ignored in this calculation which must be considered before one can determine definitely whether this population inversion is possible. The most serious defect in this calculation is that we have ignored the fact that the excited quasiparticles obey Fermi statistics. The inclusion of this restriction at these high injection levels will undoubtedly broaden the distribution of excitations, and it is incorrect to assume that all excited particles are at an energy Δ . This will result in an energy broadening of the 2Δ spike. Also, serious questions regarding the gap dependence at this high injection rate, and the value and time dependence of τ_R in this nonequilibrium situation must be precisely known. Experimentally we have so far only studied the generator-power dependence of the phonon signals in the range of pulse powers of 1 to about 40 W. The observed signal over this range is found to go up very nearly as the square of the power. This behavior is believed to be in large part due to nonlinearity in the detecting junction. A detailed investigation of possible effects due to stimulated emission is under way.

V. CONCLUSIONS

Using the stress-dependent properties of the Sb-donor levels in Ge, we have shown that the spectrum of phonons emitted from a superconducting tunnel junction into a crystal possesses a large peak at an energy value 2Δ (the superconducting energy gap.) Utilizing an identical superconductor tunnel junction as a detector the system behaves effectively as a monochromatic source. This result persists up to quite high-power levels and to explain these results it is necessary to invoke a mod-

el whereby phonons $\hbar\omega > 2\Delta$ are reabsorbed by the superconductor very quickly and the only phonons escaping are $\hbar\omega \leq 2\Delta$. This model was then applied to the situation of a heat pulse incident upon a superconducting film. We have shown that the frequency spectrum of a heat pulse can be correctly determined by properly taking into account the power generated and the specific-heat mismatch between the heater and the crystal. Utilizing this thermal spectrum, we have applied this down-conversion model to a heat pulse on various superconductors at various temperatures, and the results qualitatively agree with our experimental observations on a similar system. The black-body spectrum is transformed into a distribution displaying a large peak (as well as an upper energy cutoff) at 2Δ . The powers we have been able to generate in this peak are of the order of a watt.

In addition to displaying the flexibility of the system to the choice of superconductor (thereby varying 2Δ) we have shown that by the application of parallel magnetic field, 2Δ (and hence the emitted spectrum) can be tuned for a specific superconductor. Our results have shown that the range of this tunability is at least $\Delta < \hbar\omega < 2\Delta$ and perhaps further at sufficiently low temperatures. These two aspects of tunability render the device useful over a substantial energy range in the far-infrared region (in principle from about 0.3–3 meV).

As a result of our studies of modal and energy dependence of the absorption in Ge:Sb we have been able to draw certain conclusions about the interaction of phonons with these Sb impurity levels. By far the dominant scattering mechanism when

$\hbar\omega \approx 4\Delta_c$ is that of resonance absorption proposed by Griffin and Carruthers, while the static model, calculated by Keyes, is not significant in this energy range. We have also used the device, and the magnetic field tunability, to observe the ground-state splitting of the V^{3+} ion in Al_2O_3 occurring at 1.02 meV, and the order of magnitude estimate for the magnetoelastic coefficient G_{44} is found to be $\sim 10^{-15}$ erg.

The applicability of this technique appears to be quite widespread. Tunnel junctions can be fabricated on most solid surfaces if adequately prepared and the measurement is then limited by phonon mean-free-path considerations in the crystal under study. The variation of energy gap with material and magnetic field make possible phonon propagation and interaction studies in a frequency region heretofore most difficult to achieve.

Note added in manuscript. In a recent experiment at lower temperatures we have indeed observed the expected BCS singularity at the 4Δ rise. In addition we have seen the transition from the linear to the square-root limit²⁷ (number of injected particles \gg number of particles thermally excited). These data will be published elsewhere.

ACKNOWLEDGMENTS

We would like to thank W. F. Flood for excellent crystal polishing of our samples, M. A. Chin for invaluable technical assistance, Mrs. R. C. Fulton for some of the computations, D. D. Sell for advice and loan of apparatus, and J. M. Rowell and S. Geschwind for continued advice and interest.

¹R. C. Dynes, V. Narayanamurti, and M. Chin, *Phys. Rev. Letters* **26**, 181 (1971).

²V. Narayanamurti and R. C. Dynes, *Phys. Rev. Letters* **27**, 410 (1971).

³W. Eisenmenger and A. H. Dayem, *Phys. Rev. Letters* **18**, 125 (1967).

⁴V. Narayanamurti and R. O. Pohl, *Rev. Mod. Phys.* **42**, 201 (1970).

⁵R. J. von Gutfeld and M. Pomerantz, in *Proceedings of the Ninth International Conference on the Physics of Semiconductors*, edited by S. M. Ryvlin (Nauka, Leningrad, 1968), Vol. II, p. 690.

⁶V. Narayanamurti, *Phys. Letters* **30A**, 521 (1969).

⁷J. P. Morton and H. M. Rosenberg, *Phys. Rev. Letters* **8**, 200 (1966).

⁸D. Walton, *Phys. Rev. B* **1**, 1234 (1970).

⁹N. S. Shiren, *Phys. Rev. Letters* **17**, 958 (1966).

¹⁰C. H. Anderson and E. S. Sabisky, *Phys. Rev. Letters* **21**, 987 (1968).

¹¹D. J. Channin, V. Narayanamurti, and R. O. Pohl, *Phys. Rev. Letters* **22**, 524 (1969).

¹²K. F. Renk and J. Deisenhofer, *Phys. Rev. Letters* **26**, 764 (1971).

¹³W. J. Brya, S. Geschwind, and G. E. Devlin, *Phys. Rev. Letters* **21**, 1800 (1968).

¹⁴J. Ilukor and E. H. Jacobsen, in *Physical Acoustics*, edited by W. P. Mason (Academic, New York, 1968), Vol. V.

¹⁵R. J. von Gutfeld, A. H. Nethercot, Jr., and J. A. Armstrong, *Phys. Rev.* **142**, 436 (1966).

¹⁶R. J. von Gutfeld, in Ref. 14.

¹⁷See Refs. 6 and 15. See also W. A. Little, *Can. J. Phys.* **37**, 334 (1959); O. Weis, *Z. Angew. Physik* **26**, 325 (1969). Note that for our geometry expression (1) differs from those published by a factor of 4.

¹⁸G. F. Miller and M. J. P. Musgrave, *Proc. Roy. Soc. (London)* **A236**, 352 (1956); J. M. Andrews, Jr. and M. W. P. Strandberg, *Proc. IEEE* **54**, 523 (1966); H. J. Maris, *J. Acoust. Soc. Am.* **50**, 812 (1970).

¹⁹P. C. Kwok, *Phys. Rev.* **175**, 1208 (1968).

²⁰C. C. Ackerman and R. A. Guyer, *Ann. Phys. (N.Y.)* **50**, 128 (1968).

²¹See Ref. 20. See also T. F. McNelly *et al.*, *Phys. Rev. Letters* **24**, 100 (1970); Howard E. Jackson, Charles T. Walker, and Thomas F. McNelly, *ibid.* **25**, 26 (1970).

²²L. Tewordt, *Phys. Rev.* **127**, 371 (1962).

²³L. Tewordt, *Phys. Rev.* **128**, 12 (1962).

²⁴E. Burstein, D. N. Langenberg, and B. N. Taylor, *Phys. Rev. Letters* **6**, 92 (1961).

²⁵J. R. Schrieffer and D. M. Ginsberg, *Phys. Rev.*

Letters **8**, 207 (1962).

- ²⁶H. Kinder, K. Laszmann, and W. Eisenmenger, Phys. Letters **31A**, 475 (1970).
- ²⁷A. H. Dayem, B. I. Miller, and J. J. Wiegand, Phys. Rev. B **3**, 2949 (1971).
- ²⁸B. I. Miller and A. H. Dayem, Phys. Rev. Letters **18**, 1000 (1967); K. E. Gray, A. R. Long, and C. J. Atkins, Phil. Mag. **20**, 273 (1969).
- ²⁹A. Rothwarf and M. Cohen, Phys. Rev. **130**, 1401 (1963).
- ³⁰J. Bardeen, L. N. Cooper, and J. R. Schrieffer, Phys. Rev. **108**, 1175 (1957).
- ³¹I. A. Privorotskii, Zh. Eksperim. i Teor. Fiz. **43**, 1331 (1962) [Sov. Phys. JETP **16**, 945 (1963)].
- ³²V. M. Bobetic, Phys. Rev. **136**, A1535 (1964).
- ³³M. Tinkham, in *Low Temperature Physics (Les Houches Lectures)*, edited by C. DeWitt, B. Dreyfuss, and P. G. de Gennes (Gordon and Breach, New York, 1962).
- ³⁴W. P. Mason and H. Bommel, J. Acoust. Soc. Am. **28**, 930 (1956).
- ³⁵W. P. Mason, *Physical Acoustics and the Properties of Solids* (Van Nostrand, New York, 1958), p. 323 ff.
- ³⁶A. B. Pippard, Phil. Mag. **46**, 1105 (1955).
- ³⁷J. Bardeen and D. Pines, Phys. Rev. **99**, 1140 (1955).
- ³⁸E. A. Fagen and M. P. Garfunkel, Phys. Rev. Letters **18**, 897 (1967).
- ³⁹M. P. Garfunkel, J. W. Lue, and G. E. Pike, Phys. Rev. Letters **25**, 1649 (1970).
- ⁴⁰V. Narayanamurti, Bull. Am. Phys. Soc. **15**, 821 (1970).
- ⁴¹V. L. Ginzburg and L. D. Landau, Zh. Eksperim. i Teor. Fiz. **20**, 1064 (1950).
- ⁴²L. P. Gor'kov, Zh. Eksperim. i Teor. Fiz. **36**, 1918 (1959) [Sov. Phys. JETP **9**, 1364 (1959)].
- ⁴³D. H. Douglass, Jr., Phys. Rev. Letters **6**, 346 (1961).
- ⁴⁴R. Meservey and D. H. Douglass, Jr., Phys. Rev. **135**, A24 (1964).
- ⁴⁵I. Giaever and K. Megerle, Phys. Rev. Letters **6**, 346 (1961).
- ⁴⁶R. S. Collier and R. A. Kamper, Phys. Rev. **143**, 323 (1966).
- ⁴⁷K. Maki, Progr. Theoret. Phys. (Kyoto) **29**, 10 (1963); **29**, 333 (1963); **29**, 603 (1963); **31**, 731 (1964); K. Maki and P. Fulde, Phys. Rev. **140**, A1586 (1965).
- ⁴⁸P. G. de Gennes, Physik Kondensierten Materie **3**, 79 (1964).
- ⁴⁹A. A. Abrikosov and L. P. Gor'kov, Zh. Eksperim. i Teor. Fiz. **39**, 1781 (1960) [Sov. Phys. JETP **12**, 1243 (1961)].
- ⁵⁰S. Skalski, O. Betbeder-Matibet, and P. R. Weiss, Phys. Rev. **136**, A1500 (1964).
- ⁵¹J. L. Levine, Phys. Rev. **155**, 373 (1967).
- ⁵²J. Millstein and M. Tinkham, Phys. Rev. **158**, 325 (1967).
- ⁵³E. Fagen, J. F. Goff, and N. Pearlman, Phys. Rev. **94**, 1415 (1954); J. F. Goff and N. Pearlman, *ibid.* **140**,

- A2151 (1965); B. L. Bird and N. Pearlman, in *Proceedings of the Seventh Conference on Thermal Conductivity*, edited by D. R. Flynn and B. A. Peavy, Jr., Spec. Publ. No. 302 (National Bureau of Standards, U.S. GPO, Washington, D.C., 1968) p. 103.
- ⁵⁴J. A. Carruthers, T. H. Geballe, H. M. Rosenberg, and J. M. Ziman, Proc. Roy. Soc. (London) **A238**, 502 (1957).
- ⁵⁵P. Carruthers, Rev. Mod. Phys. **33**, 92 (1961).
- ⁵⁶R. W. Keyes, Phys. Rev. **122**, 1171 (1961).
- ⁵⁷A. Griffin and P. Carruthers, Phys. Rev. **131**, 1976 (1962).
- ⁵⁸P. C. Kwok, Phys. Rev. **149**, 666 (1966).
- ⁵⁹M. Pomerantz, Proc. IEEE **53**, 1438 (1964); Phys. Rev. B **1**, 4029 (1970).
- ⁶⁰W. Kohn, in *Solid State Physics*, edited by F. Seitz and D. Turnbull (Academic, New York, 1957), Vol. 5.
- ⁶¹P. J. Price, Phys. Rev. **104**, 1223 (1956); H. Fritzsche, *ibid.* **125**, 1560 (1962).
- ⁶²J. H. Reuszer and P. Fisher, Phys. Rev. **135**, A1125 (1964); **165**, 909 (1968).
- ⁶³H. J. McSkimin, J. Appl. Phys. **24**, 988 (1958).
- ⁶⁴C. Herring and E. Vogt, Phys. Rev. **101**, 944 (1956).
- ⁶⁵H. Hasegawa, Phys. Rev. **118**, 1523 (1960).
- ⁶⁶R. O. Pohl, in *Localized Excitations in Solids*, edited by R. F. Wallis (Plenum, New York, 1968), p. 434.
- ⁶⁷A. Abragam and M. H. L. Pryce, Proc. Roy. Soc. (London) **A205**, 135 (1951).
- ⁶⁸R. R. Joyce and P. L. Richards, Phys. Rev. **179**, 375 (1969).
- ⁶⁹B. Dreyfus and F. Zadworny, J. Phys. Radium **23**, 490 (1962).
- ⁷⁰A. M. deGoer, J. Phys. Radium **30**, 389 (1969).
- ⁷¹R. Guermeur, J. Joffrin, A. Levebut, and J. Penne, Phys. Rev. **187**, 1153 (1969).
- ⁷²R. D. Mattuck and M. W. P. Strandberg, Phys. Rev. **119**, 1204 (1960).
- ⁷³W. Dobrov, Phys. Rev. **134**, A734 (1964). See this reference for the expressions for the G tensor.
- ⁷⁴See, for example, W. Schroen, J. Appl. Phys. **39**, 2671 (1968).
- ⁷⁵J. M. Rowell and W. L. Feldmann, Phys. Rev. **172**, 393 (1968).
- ⁷⁶R. C. Dynes, J. P. Carbotte, D. W. Taylor, and C. K. Campbell, Phys. Rev. **178**, 713 (1969).
- ⁷⁷The optical lines were calibrated with x-ray fluorescence spectra by Miss D. M. Dodd (unpublished).
- ⁷⁸D. D. Sell and E. O. Kane, Phys. Rev. **185**, 1103 (1969).
- ⁷⁹This was measured independently in a tunnel junction of Al-Al₂O₃-Pb:Tl (see Ref. 76).
- ⁸⁰K. Suzuki and N. Mikoshiba, J. Phys. Soc. (Japan) **31**, 186 (1971).
- ⁸¹W. L. McMillan and J. M. Rowell, in *Superconductivity*, edited by R. D. Parks (Marcel Dekker, New York, 1969).
- ⁸²See *Superconductivity*, edited by R. D. Parks (Dekker, New York, 1969).

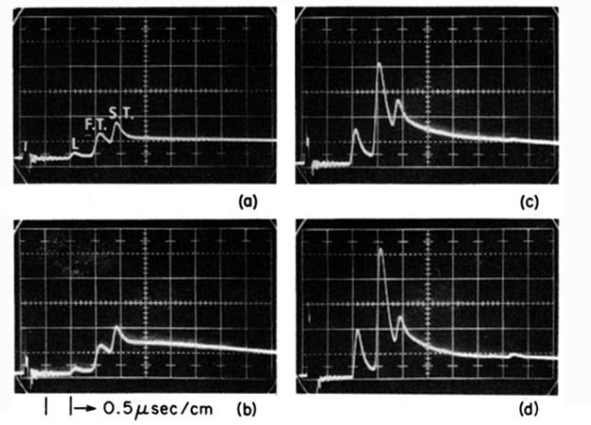


FIG. 20. Photographs of ballistic heat pulses in Ge:Sb. $N_d = 6 \times 10^{15} \text{ cm}^{-3}$. Time scale $0.5 \mu\text{sec}/\text{large division}$. Case (a) 0 stress. (b) $1.3 \times 10^8 \text{ dyn cm}^{-2}$. (c) $2.5 \times 10^8 \text{ dyn cm}^{-2}$. (d) $4.5 \times 10^8 \text{ dyn cm}^{-2}$. Path length 4.8 mm. Propagation direction $[1\bar{1}0]$. Stress direction $[111]$. Pulse power 0.4 W/mm^2 .